TIFR/TH/08-55

Heavy Ions at LHC: A Quest for Quark-Gluon Plasma

Rajeev S. Bhalerao and Rajiv V. Gavai[a]

[a]Department of Theoretical Physics, Tata Institute of Fundamental Research,
Homi Bhabha Road, Mumbai 400005, India.

Quantum Chromo Dynamics (QCD), the theory of strong interactions, predicts a transition of the usual matter to a new phase of matter, called Quark-Gluon Plasma (QGP), at sufficiently high temperatures. The non-perturbative technique of defining a theory on a space-time lattice has been used to obtain this and other predictions about the nature of QGP. Heavy ion collisions at the Large Hadron Collider in CERN can potentially test these predictions and thereby test our theoretical understanding of confinement. This brief review aims at providing a glimpse of both these aspects of QGP.

1. Introduction

There are two very commonly quoted motivations for the upcoming Large Hadron Collider (LHC) at CERN in Geneva, the center of attraction for the articles in this volume. Perhaps the primary one is that LHC will provide us a key to understand the origin of the visible mass of our Universe. This alludes to that fact that our standard model(SM) of particle interactions has to start with matter in the form of massless quarks and leptons. The famous Higgs mechanism [1] of spontaneous breaking of gauge symmetries provides masses to them, and the carriers of the weak force, namely $W^{\pm}$, Z. LHC is widely expected to discover the Higgs boson which is tied with this mechanism. The other motivation rests on the fact that the standard model has been well understood due to the many impressive precision tests carried out in many experiments, including those at the Large Electron Positron (LEP) at CERN and the Tevatron at the Fermilab in the USA. However, new physics beyond the standard model (BSM) has to exist [2] since SM contains many, at least 19, arbitrary parameters and thus cannot be the final theory. Indeed, it is even hoped that LHC may provide us not only a glimpse of the BSM physics, but it will hopefully also explain the origin of the mass of the dark matter in the Universe.

While these motivations are largely correct, there are certain oversimplifications in them, leading to a few misconceptions, especially in the popular media. First of all, even if the expected Higgs particle is actually discovered, the origin of the mass of up/down (u/d) quarks can be claimed to be understood only after it is also established that the Higgs particle couples to them with a strength of $\sim 10^{-6}$, not an easily achievable goal at LHC. Indeed, one may as well need an electron-positron collider to establish this in the post-LHC era. Moreover, the protons and neutrons, which make up most of the visible mass in our Universe, have each a much larger, almost a factor of 100 larger, mass than the sum of the masses of their constituent u/d quarks. Therefore, the understanding of the visible mass of the Universe will emerge from the efforts to figure out why protons/neutrons have such large binding energies. Starting from molecules to atoms and nuclei, we are accustomed to the idea that the interactions which bind the respective constituents give rise to binding energies much smaller, less than even a per cent. This has given rise to the very successful idea of treating these interactions perturbatively as an expansion in the strength of the interaction. As we shall see below, one needs new suitable techniques to investigate these large binding energies, in Quantum Chromo Dynamics (QCD), the theory of interactions of quarks with gluons, the carriers of the strong force.

As may be seen from the articles in this volume itself, QCD is an integral part of our standard model of particle and their interactions. From various experiments in the past, it is well known that quarks carry both flavour quantum numbers such as, electric charge or strangeness, as well as colour: they transform as a triplet under the colour SU(3) group. As in the case of electric charge, the colour charge is also mediated by massless vector particles, gluons. Structurally, the theory of quark-gluon interactions, QCD, looks very similar to that of electron-photon interactions, QED. A key difference though is that there are eight gluons which themselves carry colour charge, transforming as an octet under SU(3)-colour group. Consequently, gluons can interact amongst themselves. Furthermore, the QED coupling is rather small at the scales we probe, being 1/137, whereas the smallest measured QCD coupling, α_s, is about 0.12. In fact, more often, one has to deal with $\alpha_s = 0.3$ or so and it is > 1 in the bound states like proton or neutron. QCD exhibits a much richer structure and a variety of phenomena as a result of this large α_s. Quark confinement and dynamical chiral symmetry breaking can be named as typical examples. A lack of observation of quarks in experiments led to the hypothesis that quarks are permanently confined in the hadrons, i.e, protons or pions whereas the lightness of pions compared to protons is expected to be understood as the phenomenon of dynamical breaking of the chiral symmetry by the vacuum. QCD as the theory of strong interactions has to explain these phenomena. Since, QCD is too complex, simple models based on underlying symmetries are often employed to account for its non-perturbative aspects. Indeed, most, if not all, of the "precision tests" are either performed experimentally only at small coupling, α_s, corresponding to rather rare events, or employ the simple QCD-based models. The latter are in many cases possible weak links in the precision tests of the standard model : physics beyond standard model may even show up in non-perturbative QCD beyond these models. We need to look for it and rule out such a mundane possibility for BSM-physics in order to be sure that other exotic possibilities are indeed worth looking for. Thus, non-perturbative techniques are needed for real precision tests of QCD. As a glaring example, let me mention that the easiest precise measurement at LHC will perhaps be the total proton-proton cross section at 14 TeV. The current best theoretical prediction for it is [3] $\sigma^{tot} = 125 \pm 25$ mb ! As explained in [3], one uses the so-called Regge Models to arrive at it, and one such model can even explain the currently observed Q^2-variation of the structure function of proton, F_2, as well. Recall that a key cornerstone for establishing QCD as the theory of strong interaction is this Q^2 variation.

While obtaining a reliable prediction for the above cross section from QCD still seems far away, a non-perturbative technique does exist today to obtain other quantities, such as the decay constants or the weak matrix elements, from QCD using first principles, and these could still provide non-perturbative precision tests of the standard model. QCD defined on a space-time lattice is such a tool. Not only does it explain many of the above mentioned phenomena but it provides quantitative estimates of many physical observables. Furthermore, the same techniques of lattice QCD lead to spectacular predictions for the behaviour of matter under extreme conditions. Thus, lattice QCD predicts the existence of a new phase, called Quark-Gluon Plasma (QGP) at sufficiently high temperature, and a phase transition of the strongly interacting matter of protons, neutrons and pions to the new phase QGP at high enough temperature. The dynamically broken chiral symmetry of QCD at low temperatures in our world is expected to be restored in the QGP phase, 'melting' away the constituent mass of the light quarks acquired due to interactions.

Our Universe ought to have existed in such a phase a few microseconds after the Big Bang, and about 20 microseconds later the phase transition to the normal hadrons like protons, neutrons and pions ought to have taken place in it. Whether there are any imprints of this phase transition on the astronomical objects observed today depends on the nature of the phase transition. There have been speculations of stars with strange matter, consisting of neutral baryons made from an up, down and a strange quark each. Similarly attempts have been made to study the influence of such a phase transition on the Big Bang Nucleosynthesis. More excitingly, the Large Hadron Collider (LHC) itself will provide us with an opportunity to create these Early Universe-like conditions of high energy densities, or equivalently high temperature, in the laboratory in its proposed heavy ion collisions of Lead on Lead at 5.5 TeV colliding energy. Heavy ion collisions at relativistically high energy have had an illustrious past, and even more impactful present. Early such experiments were made at the SPS collider in CERN, Geneva at a colliding energy of 17 GeV per nucleon in the center of mass (cm) frame. The relativistic heavy ion collider (RHIC) has been operative in BNL, New York, since a last few years and has produced heavy ion collision data for a variety of ions, Deuterium (D), Copper(Cu), and Gold (Au), at a spectrum of energies, 62–200 GeV per nucleon in the cm frame. Experiments at LHC will thus see a further jump in the colliding energy by a factor of about 30. It is hoped that this will offer us cleanest environment yet for investigating the physics of quark-gluon plasma.

In this short review, we shall attempt to provide a glimpse of how lattice QCD leads to QGP and predicts many of its properties as well as those of the corresponding phase transition and how the heavy ion collision experiments amazingly provide us an opportunity to produce QGP in a laboratory, including the expectations of what we may observe at LHC.

2. QGP from Lattice QCD

In order to understand and appreciate the fundamental importance of attempts to discover QGP at the LHC, let us first review the basics of lattice QCD and why it facilitates a truly reliable treatment of non-perturbative physics. In the process, we shall also see why essentially the same tested technique for obtaining, say, the hadron masses, comes into play for predicting new phases or phase transitions.

2.1. Basic Lattice QCD

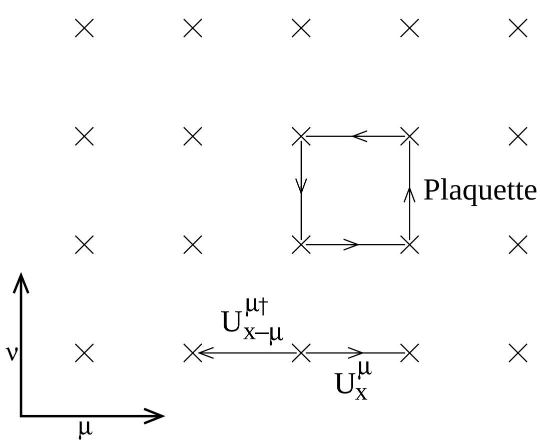

Figure 1. Quark and gluon fields on a space-time lattice.

Lattice field theory is defined by discretizing the space-time. The (inverse of the) lattice spacing a acts as the ultra-violet cut-off needed to tame the divergences in a quantum field theory. One places the anti-commuting quark fields $\psi(x)$, and $\bar\psi(x)$ on lattice sites whereas the gluon fields reside on the links, as shown in Figure 1. A directed link from site x in the positive direction $\hat\mu$ is associated with the gluon field U^μ_x, while the link to the site $x-\hat\mu$ in the opposite direction is $U^{\mu\dagger}_{x-\hat\mu}$. A gauge transformation $V_x \in SU(3)$ rotates the quark field in the colour space: $\psi'(x) = V_x\,\psi(x)$. Demanding that the gluon field at the link x in the direction $\hat\mu$, $U^\mu(x)$, change to $U'^\mu(x) = V_x U^\mu(x) V^{-1}_{x+\hat\mu}$, ensures that the (discrete) kinetic energy term of quarks remains invariant under such a gauge transformation. Constructing gauge actions from closed Wilson loops of the links, like e.g., the smallest square loop, called plaquette and displayed in Figure 1, ensures their gauge invariance.

It turns out that a straightforward discretization of the derivative, given by $[a\,\partial\psi(x) = \psi(x+a\hat\mu) - \psi(x-a\hat\mu)]$, can be made gauge invariant as shown in the Figure 1, where the links end on respective quark fields at the sites. Thus a sum over all independent terms of both types shown in Figure 1 yields the QCD action on the lattice. However, it leads to the so-called Fermion Doubling problem: each lattice fermion corresponds to $2^d = 16$ flavours in the continuum limit of $a \to 0$. Various lattice Fermion actions, referred to as the Staggered, Wilson, Domain Wall or Overlap Fermions, have been proposed to alleviate this problem. In view of their simplicity and an exact chiral symmetry even on the lattice, the staggered Fermions have dominated the field of interest for this article, namely lattice QCD at finite temperature and density. Briefly, these are single component Grassmann variables on each site, with the γ-matrices replaced by suitably defined sign factors. They have a $U(1)\times U(1)$ chiral symmetry and 4 flavours in continuum limit. An oft-discussed problem of the staggered Fermions, though, is that two or three light flavours are not simple to define, and the currently used methods may miss out on important physics aspects related to anomalies. It is often argued that for the bulk thermodynamic properties these issues are likely to be unimportant.

Typically, for any lattice computation one needs to evaluate the expectation value of an observable Θ,

$$\langle\Theta(m_v)\rangle = \frac{\int DU\,\exp(-S_G)\,\Theta(m_v)\,\mathrm{Det}\,M(m_s)}{\int DU\,\exp(-S_G)\,\mathrm{Det}\,M(m_s)}\;; \qquad (1)$$

where M is the Dirac matrix in x, colour, spin, flavour space for sea quarks of mass m_s, S_G is the gluonic action, and the observable Θ may contain fermion propagators of mass m_v. $S_G \sim 6\sum_P \mathrm{tr}U_{plaq}/g_0^2$, with g_0 the bare coupling and U_{plaq} the product links along a plaquette as shown in Figure 1. Amongst the many methods of evaluation of eq.(1), numerical simulations stand out due to the ability to achieve the goal of removing the lattice scaffolding, i.e., taking the continuum limit $a \to 0$. Using the two-loop β-function, it is easy to show that

$$M\cdot a = \frac{M}{\Lambda_L}\,(g_0^2 b_0)^{-b_1/2b_0^2}\, e^{-\frac{1}{2b_0 g_0^2}}\,(1+O(g_0^2))\;; \qquad (2)$$

defines the way a mass scale $M\cdot a$ on the lattice changes as the bare coupling $g_0\,(=\sqrt{6/\beta})$ is changed. Here b_0 and b_1 are the universal coefficients of the β-function. Typically, one needs larger and larger lattice sizes as $a \to 0$ in order to keep physical volume fixed.

Numerically, the $\langle\Theta\rangle$ is computed by averaging over a set of configurations $\{U^\mu(x)\}$ which occur with probability $\propto \exp(-S_G)\,\mathrm{Det}\,M$. Thus the main problem is to generate the ensembles of such configurations with the desired probability distribution. Complexity of evaluation of $\mathrm{Det}\,M$ has lead to various levels of approximations in the process of generation of configurations: the quenched approximation consists of sea quark mass, $m_s = \infty$ limit whereas the full theory should have low sea quark masses: $m_u = m_d$ with a moderately heavy strange quark. The computer time required to obtain results at the same precision increases as the sea quark mass is lowered.

2.2. Some Results from Lattice QCD

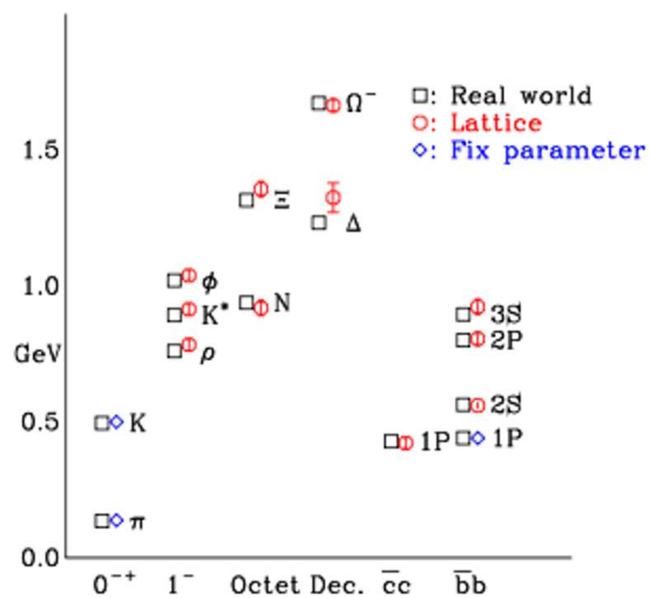

Figure 2. Comparison of experimental hadron spectra with lattice results [4].

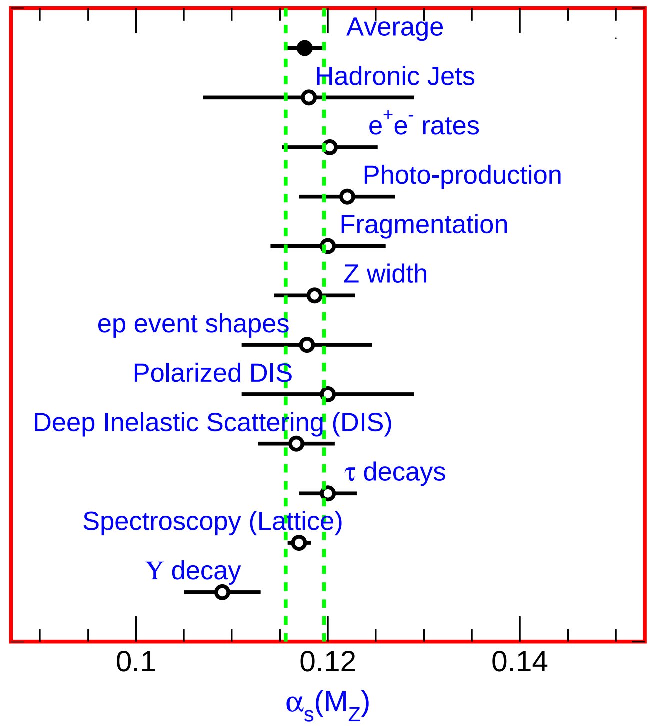

Figure 3. Various determinations of $_s$. From [5].

A variety of qualitative and quantitative results have been obtained using the lattice techniques. It will be both impractical and unnecessary to review all of them here. However, in order to appreciate the power of these techniques, we limit ourselves to providing a glimpse of them for the staggered fermions; similar, sometimes better in quality/precision, results have been obtained with the Wilson fermions as well. Figure 2 shows [4] the results of the MILC and HPQCD collaborations for the light as well as heavy hadrons obtained with light sea quarks. Using the pion and kaon masses to x the scales of the corresponding quark masses, most other particle masses are found to be in good agreement with the experiment. Furthermore, the spontaneous breaking of the chiral symmetry has been demonstrated by many groups since the early days of the lattice QCD, showing a non-vanishing chiral condensate, h i ≠ 0. Moreover, the goldstone nature of the pion has also been veri ed by checking that m^2 / m_u. Figure 3 displays a comparison [5] of the lattice determination of the strong coupling, $_s(M_Z)$, with other perturbative determinations from experimental data. While these results verify that QCD is indeed the correct theory of the strong interactions, and the lattice technique is the most reliable quantitative tool to extract its non-perturbative properties, making new predictions for the experiments is where the real challenges and excitement lies. It is very heartening to note that the decay constants of pseudo-scalar mesons containing a heavy quark were rst obtained using lattice techniques: $f_{D^+} = 201 \;\; 3 \;\; 17$ MeV and $f_{D_s} = 249 \;\; 3 \;\; 16$ MeV [6]. These have since been measured experimentally to be $f_{D^+} = 223 \;\; 16 \;\; 7$ MeV [7] and $f_{D_s} = 283 \;\; 17 \;\; 14$ MeV [8], in excellent agreement with the lattice QCD predictions.

2.3. Lattice QCD at Nonzero Temperature and Density

Investigations of QCD under extreme conditions, such as high temperatures and/or densities, provide a solid platform for its most spectacular non-perturbative tests. Since the results from hadron spectroscopy x the quark masses as well as the scale $_{QCD}$, these tests are even completely free of any arbitrary parameters. Based on simple models, which build in the crucial properties of con nement or chiral symmetry breaking and allow asymptotically for the free quark gluon gas, one expects phase transitions to new phases such the Quark-Gluon Plasma or the colour superconductors. As we shall see in the next section, the experimental possibilities of creating the required temperature, and thus the new QGP phase, exist in the heavy ion collisions at high energies in BNL, New York and CERN, Geneva. Considering the scale of the entire experimental enterprise, both in man-years invested and money spent, it seems absolutely necessary to have a better theoretical foundation for these results compared to merely relying on simple models. Fortunately, one can use the canonical Euclidean field theory formalism for equilibrium thermodynamics to look for the new phases, and the phase transitions in ab initio calculations from the underlying field theory, i.e., QCD. Indeed, properties of the QGP phase can be predicted theoretically using the lattice QCD approach, and tested in the experiments at BNL and CERN. As a first principles based and parameter-free approach, Lattice QCD is an ideal reliable tool to establish the QCD phase diagram and the properties of its many phases. While most other basic features of the lattice formalism required for such an exercise remain the same as in section 2.1, a key difference for simulations at finite temperature is the need of an $N_s^3 \times N_t$ lattice with the spatial lattice size, $N_s \gg N_t$, the temporal lattice size for the thermodynamic limit of $V = N_s^3 a^3 \to \infty$. The temperature $T = 1/(N_t \cdot a)$ provides the scale to define the continuum limit: Fixing the transition temperature in physical (MeV) units and using eq. (2), the continuum limit is obtained by sending $N_t \to \infty$.

The lattice QCD approach has provided information on the transition temperature, the order of the phase transition, and the equation of state of QCD matter. One exploits the symmetries of the theory to construct order parameters which are then studied as a function of temperature to look for phase transitions, if any. QCD has two different symmetries in opposite limits of the quark mass m_q. For N_f flavours of massless quarks, QCD has $SU(N_f) \times SU(N_f)$ chiral symmetry while for $m_q \to \infty$, it has a global $Z(3)$ symmetry. Such symmetries usually imply zero expectation values for observables which transform nontrivially under it unless the symmetry is broken spontaneously due to dynamical reasons and the vacuum transforms nontrivially under it. Lattice techniques enabled us to establish that the chiral symmetry is broken spontaneously at low temperatures, as indicated by its non-vanishing order parameter, the chiral condensate $\langle\bar\psi\psi\rangle \neq 0$. Its abrupt restoration to zero at high temperature will be a signal of a chiral symmetry restoring phase transition. Since the chiral condensate can be regarded as an effective mass of a quark, arising due to QCD interactions, the chiral transition can be interpreted as thermal effects 'melting' this mass. Similarly, the global $Z(3)$ symmetry breaking can be shown to be equivalent to a single quark having a finite free energy, i.e., the existence of a free quark. A nonzero expectation value for its order parameter, the Polyakov loop $\langle L \rangle$, is the a signal for deconfinement. Of course, in our world with two light and one moderately heavy flavours, neither symmetry is exact but these order parameters may still act as beacons for transitions, depending on how mildly or strongly broken they are.

2.4. Results from Lattice QCD at $T \neq 0$.

The transition temperature T_c can be determined by locating the point of discontinuity or sudden change in the order parameter as a function of the temperature (or other external parameter such as density). Since numerical results are necessarily obtained on finite lattices, there is an inevitable rounding which makes the determination of T_c a little tricky. A lot of work has been done on this question in the statistical mechanics area and standard finite size scaling techniques exist to pin down T_c as well as the order of the transition. Since the early days, numerical simulations of lattice QCD have progressively tried to approach the real world of light quarks with vanishing effects from the lattice cut-off. The efforts began from the quenched approximation, i.e., QCD without dynamical quarks, where the deconfinement order parameter $\langle L \rangle$ on small N_t-lattices was used to establish a first order deconfinement phase transition. Later QCD with three or more light dynamical quarks was also shown to have a first order chiral transition. Recent work on simulations for QCD with a realistic quark spectrum seems [9] to rule out a first order chiral transition or a second order transition with the expected O(4)-exponents, but suggests a rapid cross over. Determination of T_c, now the point of sharpest change, is even more tricky as a result. The current range for it can be summarized to be 170–190 MeV. A value on the lower end of the range was obtained [10] by using larger N_t-lattices while a value at the upper end was obtained [11] using improved action but smaller N_t. There are other technical differences, such as the physical observable used to set the scale of lattice QCD, as well. Since the energy density is proportional to T^4, the current uncertainty in the value of T_c translates to a $\sim 60\%$ difference in the corresponding energy density estimates at T_c. In view of the tremendous impact it has on the requirements of heavy ion collision experiments, it is hoped that a narrowing of the range takes place as a result of future lattice QCD work.

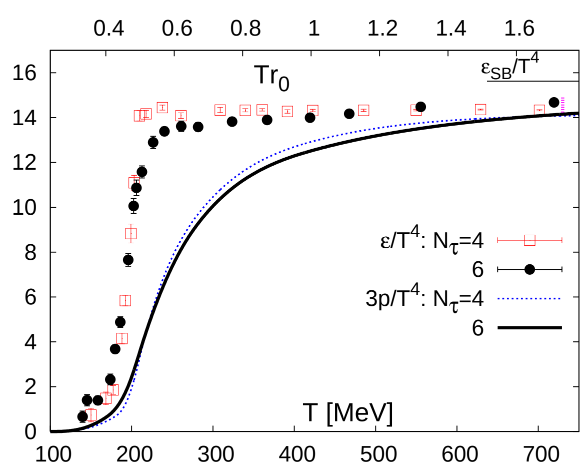

Figure 4. Energy density and Pressure from lattice QCD. Taken from [12].

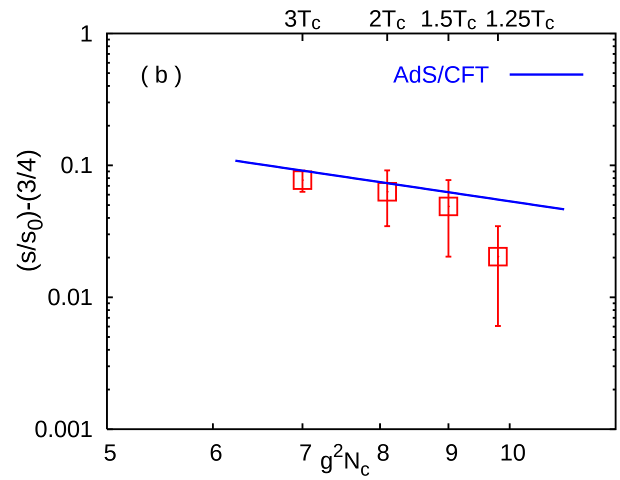

Figure 5. Entropy density s (in units of ideal gas entropy s_0) as a function of 't Hooft coupling. From [13].

Quantities of thermodynamic interest such as the energy density, or the pressure or various quark number susceptibilities can be obtained by using the canonical relations from statistical mechanics. Thus,

$$\varepsilon = \frac{T^2}{V}\left(\frac{\partial \ln Z}{\partial T}\right)_{V,\mu} \quad \text{or} \quad \chi_B = \frac{T}{V}\left(\frac{\partial^2 \ln Z}{\partial \mu_B^2}\right)_{V,T}; \text{ etc.} \quad (3)$$

Early results in the quenched QCD showed the existence of a QGP phase which has energy density of about 85 % of the corresponding ideal gas. The progress since then has been in employing large N_t and inclusion of light quark loops. Figure 4 displays recent results from such efforts. Obtained on two different lattice sizes, N_t = 4 and 6 with nearly realistic u,d and s masses, these results also exhibit similar kind of, ∼ 15% , deviations from the ideal gas and do seem to hint towards the lattice cut-off effects to be small. The spatial volumes are perhaps not large enough to ensure that the thermodynamic limit is reached. However, this question is likely be addressed in near future soon. The results also suggest at most a continuous transition or even a rapid cross over; a strong first order phase transition assumed/constructed in many phenomenological models seems clearly ruled out. This has implications for the hydrodynamical models used to analyse the experimental data: possible mixed state of quark-gluon plasma and hadronic gas must be short lived, if at all it exists.

From a theoretical perspective investigation of equation of state offers hints of developing analytic or semi-analytic approaches. Thus conformal invariant theories are known to yield a variety of predictions for the thermodynamic quantities using the famous AdS-CFT correspondence. Figure 5 shows an attempt to confront the entropy density [13] for the quenched QCD in terms of the entropy of the ideal gas with the prediction of $\mathcal{N}$ = 4 SYM [14]. The agreement is impressive, considering the differences of the underlying theories. On the other hand, it is really in the stronger coupling region that it is not as good. Moreover, resummed weak coupling perturbation theory approaches seem to perform equally well at the lower couplings. Figure 6 shows the results [13] for the equation of state to highlight how conformal QCD really is. The ellipses denote 66% error bounds on the measured EOS. The wedges piercing the ellipses have average slope c_s^2, the speed of sound and the opening half-angle of these wedges indicate the error in c_s^2. Conformal invariance is indeed violated significantly in the region close to the transition, with least violation at the same temperatures where in AdS-CFT prediction does well in Figure 5.

Viscosities of the quark-gluon plasma, both the shear (η) and bulk (ζ), can also be determined using the lattice approach although unlike the equation of state these determinations need extra ansatze some of which are not universally accepted. Kubo's linear response theory lays down the framework to obtain such transport coefficients from certain equilibrium correlation functions. In particular, one obtains correlation functions of energy-momentum tensor using the lattice approach above. These are, of course, defined at discrete Matsubara frequencies. Recall that the simulations at $T \neq 0$ need lattices with i) periodic boundary condi-

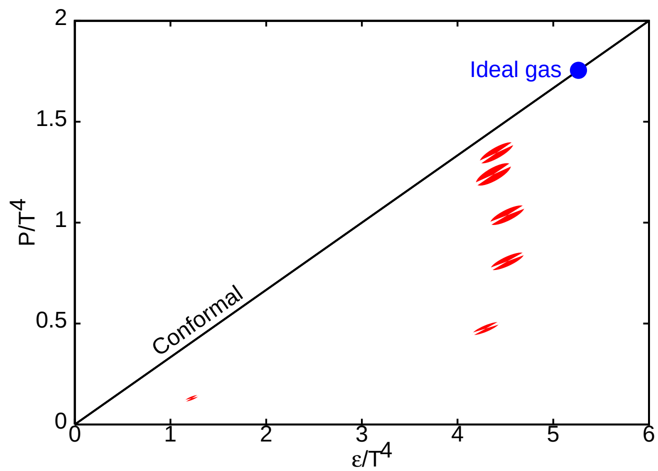

Figure 6. Equation of State for (quenched) lattice QCD. Taken from [13].

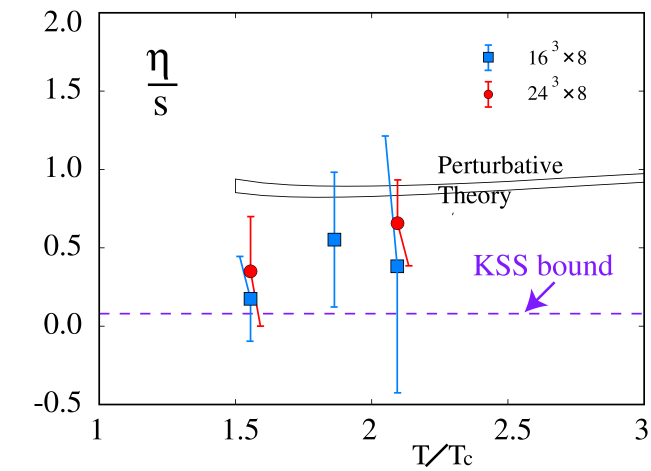

Figure 7. Ratio of shear viscosity to entropy in (quenched) QCD vs. temperature. Taken from [15].

tions and ii) small N_t compared to N_s. The correlation function is thus de ned at few discrete points only. One then continues it analytically to get the so-called retarded propagators in real time from which the the and are obtained in the zero frequency limit. Figure 7 shows the results [15] in the quenched approximation. Close to T_c, rather small values are obtained for the ratio of to the entropy density s. These are seen to be consistent with the famous bound [16] from AdS-CFT. As shown in the Figure, perturbation theory suggests rather large values for this ratio. These results have since been re ned [17] and made more precise but the general picture remains the same, as do the various theoretical uncertainties which plague these determinations. Larger lattices and inclusion of dynamical quarks will surely reduce some of these in near future. What is needed though for a more convincing demonstration of the fact the shear viscosity is indeed as small as hinted by the experimental data (see the next section) is a better control over the systematic errors in the analytic continuation.

Analogous to the baryon number susceptibility, de ned in eq. (3), various quark number susceptibilities can be de ned by taking derivatives with the appropriate chemical potential. These determine the uctuations in the given conserved quantum number, say, strangeness. It has been argued [18] that under certain assumptions, testable experimentally, the strange susceptibility can be related to the Wroblewski parameter $_s$ extracted from the data of heavy ion collisions. Interestingly, lattice QCD computation in both quenched approximation and full QCD yield a $_s(T_c) ' 0.4$ 0.5, whereas various experimental results [19] lead to a value 0.47 0.04. Taking derivatives with two di erent chemical potentials in eq. (3), one obtains o -diagonal susceptibilities. These have the information on avour correlations. Such a baryon-strangeness [20] or electric charge-strangeness [18] correlation has been proposed as a signature for identifying the nature of the high temperature phase as that of the quark-gluon phase.

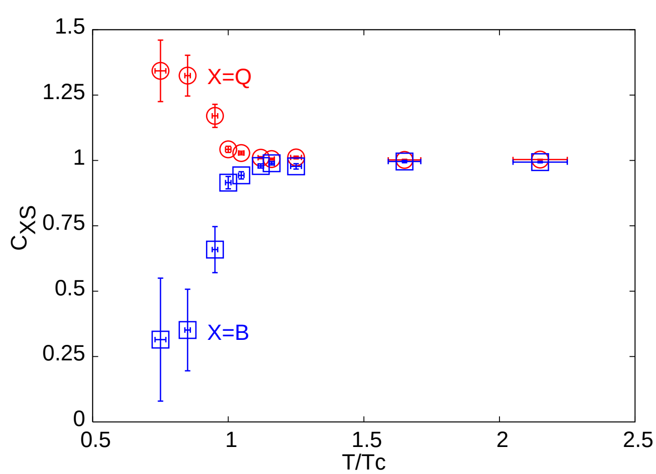

Figure 8. Baryon-Strangeness and Electric charge-Strangeness correlation vs. temperature [18].

Figure 8 shows the lattice results for QCD with 2 light dynamical quarks for both these correlations. They have been so normalized that a value unity, as seen in most of the high temperature phase in Figure 8, characterises the existence of quark degrees of freedom with the appropriately fractional baryon number or charge. It has been shown that the correlation in the low temperature phase are consistent with the hadronic degrees of freedom. Indeed, any lack of the expected transition should lead to much milder temperature dependence as well as a value di erent from unity for these correlation functions. Being ratios of the quark number susceptibilities, these correlations are robust, both theoretically and experimentally. Systematic errors due to lattice cut-o or dynamical quark masses are therefore very small as are the systematic errors from experimental sources.

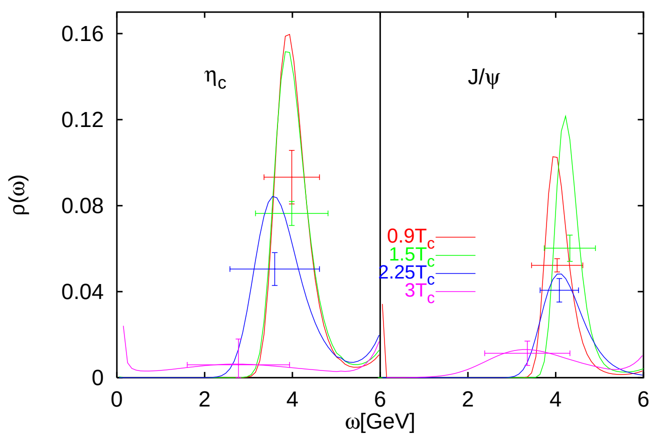

Figure 10. Spectral function of $_c$ and J= . From [22].

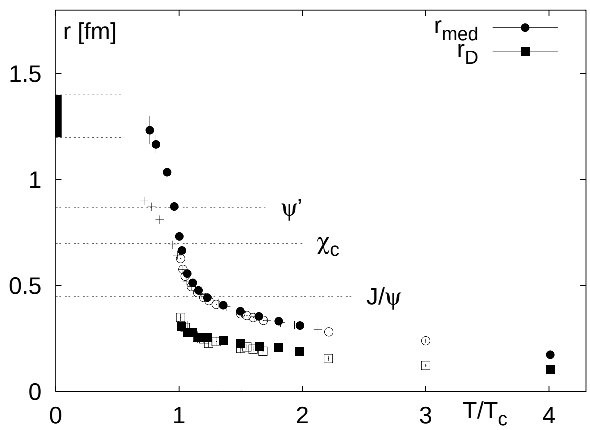

Figure 9. Debye radii for charmonia vs. temperature[21].

Debye screening of coloured heavy quarks in the decon ned phase had long been recognised [23] as a possible signal of formation of quark-gluon plasma, detectable in the suppression of heavy quarkonia in the heavy ion collisions. In view of the impressive data from CERN at lower SPS energies, and the expectations from the upcoming LHC experiments, a critical assessment of the original theoretical argument seems prudent. Lattice QCD has contributed handsomely in nite temperature investigations of both the heavy quark-antiquark potential, which can be used in the Schrodinger equation to look for the melting of heavy quarkonia, and directly in the spectral function at nite temperature. Figure 9 displays the results [21] for the screening radii estimated from the inverse non-perturbative Debye mass m_D in quenched (open squares) and full (lled squares) QCD. For $r < r_{med}$, the medium e ects are suppressed, leading to the same heavy quark potential as at $T = 0$. The horizontal lines correspond to the mean squared charge radii of J= , $_c$ and 0 charmonia, and are thus the averaged separations r entering the e ective potential in potential model calculations. Figure 9 therefore suggests that the $_c$ and 0 states would melt just above the transition while J= may need higher temperatures to be so a ected. Direct spectral function calculations [22] provide a strong support for such a qualitative picture. Such computations have been made feasible by the recognition of the maximum entropy method (MEM) technique as a tool to extract spectral functions from the temporal correlators computed on the Euclidean lattice. However, as in the case of shear viscosity above, the data for such temporal correlators are sparse, making the extraction more of an art. Nevertheless, large lattices, 48^3 12 to 64^3 24 have been used in this case to avoid such criticisms. Figure 10 shows typical results for the J= and $_c$ mesons in the quenched approximation. The vertical error bars denote the possible uncertainties on the area under the peak as de ned by the horizontal error bar. The peaks in both spectral functions appear to persist up to 2.25 T_c, i.e., have nonzero area within the computed error-band, and are gone by $3T_c$ unlike the $_c$ which has no peak already by 1.1 T_c. Further technical improvements, such as the inclusion of light dynamical quarks, are clearly desirable. Another important issue is that of the huge widths of the peak compared to their known zero temperature values. If real, they could hint at rather loosely bound states which could be dissociated by thermal scatterings.

2.5. QCD Phase Diagram

The quark-gluon plasma phase and the corresponding quark-hadron transition which we discussed so far is a special case of the conditions that could be created in the heavy ion collisions. Indeed, the lattice QCD thermodynamics that we considered was for the case of zero net baryon density and an almost baryon-free region can be produced in the heavy ion collisions in the so-called central rapidity region, as we explain in the next section. It also pervaded our Universe a few microseconds after the Big Bang. In general, of course, one should expect hot regions with some baryon number since the colliding nuclei themselves carry substantial baryon number. Massive stars could also have regions of huge baryon densities in the core which could even be at rather low temperatures. It is natural to ask what these generalized extreme conditions lead us to. One could have new phases, and different natures of phase transitions which may even have astrophysical consequences. The vast research area of QCD phase diagram in the plane of temperature T and the baryonic chemical potential μ_B deals with these and several other interesting issues. While the current theoretical expectations suggest such physics at nontrivial baryon densities to be better accessible to the colliders at lower energies, such at the RHIC in New York or the forthcoming FAIR facility at GSI, Darmstadt, we feel that the physics may be interesting in its own right to be included in this article dedicated to LHC; with some luck LHC experiments may have important contributions to this area as well.

Using simple effective QCD models, such as the Nambu-Jana Lasinio model at finite temperature and densities [24], several speculations have been made about how the QCD phase diagram in the $T-\mu_B$ plane should be. At asymptotically high densities, one expects quarks to be effectively free, and therefore to exhibit various colour superconducting phases [25]. In the limit of large number of colours N_c for quarks, it has also been argued that a “quarkyonic” phase may exist [26] at low enough temperatures. A crucial question, especially in the context of either the massive stars, or heavy ion collisions, is the quantitative reliability of the predicted regions in the $T-\mu_B$ space. Alternatively, it is unclear how low can the asymptotic predictions be trusted. Nevertheless, most model considerations seem to converge [25] on the idea of the existence of a critical point in the $T-\mu_B$ plane for the realistic case of 2 light flavours ($m_u = m_d$) of dynamical quarks with a moderately heavy strange quark. Establishing it theoretically and/or experimentally would have huge profound consequences in our (non-perturbative) understanding of QCD.

Extending the lattice approach to the case of QCD at finite density has turned out to be a challenging task at both conceptual and computational level. In principle, it really is straightforward. One just has to add a term $\mu_B N_B = \mu_B \bar{\psi}\gamma_0\psi$ term to the fermionic part of the action, hence the Dirac matrix M, in eq.(1). In order to eliminate certain spurious divergences, even in the free case, some care is needed [27] and the naive form above has to be modified. A big conceptual block has, however, turned up in form of our inability to define exact chiral invariance in the presence of the chemical potential [28]: both the Overlap and the Domain Wall fermions lose their exact chiral invariance for any nonzero μ. The staggered fermions do preserve the chiral invariance for nonzero μ. Furthermore, they are simpler to handle numerically. Again most of the numerical work has therefore employed the staggered fermions, although they are plagued with the difficulties of precise definition of flavour and spin as mentioned earlier. Indeed, the existence of the critical point depends [25] crucially on how many flavours of light quarks the theory has. Proceeding none the less with the staggered quarks, another tough problem arises in form of the fact that the Det M ($\mu \neq 0$) in eq. (1) is complex whereas the numerical methods of evaluation, employed to obtain the results in the sections above, work only if the determinant is positive definite. This is akin to the sign problem well known to the statistical physicists and is largely unsolved in its full generality.

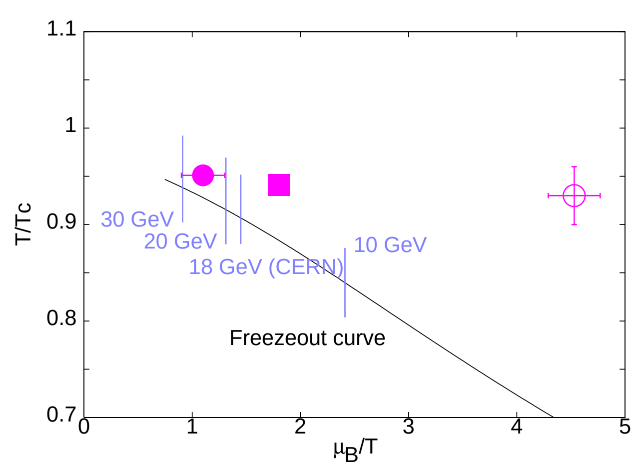

Figure 11. QCD Phase diagram for 2 light flavours of quarks. The circles [29, 31] and the square [32] denote the location of the critical point on lattices with 1/4T and 1/6T cut-offs respectively. Taken from [31], where more details can be found.

A bold breakthrough was achieved [29] by applying the method of re-weighting in the vicinity of the finite temperature transition at $\mu = 0$. A flurry of activity saw many new methods emerge [30], such as analytic continuation of computations at imaginary chemical potential and Taylor series expansions of the free energy. These have been employed to get a glimpse of whether a critical point does exist, and if yes, what its location may be. The field is really in its infancy and unfortunately at present no consensus amongst the results obtained so far has emerged. Figure 11 exhibits the results obtained for the critical point for the case of two flavours of light quarks with a pion mass $m_\pi/m_\rho = 0.31 \pm 0.01$, compared to 0.18 in the real world. The results [29, 31] denoted by circles in the Figure 11 are for a lattice cut-off $a = 1/4T$ whereas the square [32] denotes the first attempt towards the continuum limit by lowering a to $1/6T$. Large finite volumes have been observed. The shift in the location of the open circle in the Figure 11 was shown [31] to be due to the use of a 10 times larger volume than the open circle [29]. In order to be brief, we prefer to close this section by noting that different results have been claimed in the literature for larger pion masses and for a different number of flavours. It is hoped that a clear and solid picture will emerge in the near future.

3. Relativistic Heavy-Ion Collisions

At energies of a few GeV/N to a few 10's of GeV/N, colliding nuclei tend to stop each other thereby forming a dense, baryon-rich matter. At higher energies, they nearly pass through each other forming a dense, nearly baryon-number-free matter in the mid-rapidity region. This is evident in the shapes of rapidity distributions (dN/dy vs y) of the net proton (i.e., proton $-$ antiproton) production observed at various beam energies. This apparent transparency of nuclear matter at ultra-relativistic energies can be understood in the space-time picture of the collision, proposed by Bjorken [33, 34].

3.1. Bjorken Picture

Consider, for simplicity, a central (i.e., head-on or zero impact parameter) collision of two identical spherical nuclei in their CM frame. Coordinate axes are chosen such that the two nuclei approach each other along the z-axis and collide at the origin at time $t = 0$. Deep inelastic scattering experiments have revealed the parton structure of hadrons: In the proton, e.g., the valence quark distributions $xu_v(x); xd_v(x)$ peak around $x \approx 0.2$ and vanish as $x \to 0/1$. (x is the Bjorken scaling variable.) The gluon and sea quark distributions, $xg(x); xu_s(x); xd_s(x)$, on the other hand, shoot up as $x \to 0$. These numerous low-momentum partons are called wee partons. As a result of the Lorentz contraction, the longitudinal (i.e., parallel to the beam axis) spread of the valence quark wave function is reduced to $\sim 2R/\gamma$ where R is the nuclear radius and γ its Lorentz factor. However, no matter how high the beam energy (or γ), the incoming nuclei always have in them wee partons with typical momenta $p \sim \Lambda_{QCD}$, and hence longitudinal spread ~ 1 fm [33]. The wee partons prevent the nucleus from shrinking below ~ 1 fm in the z-direction. If $2R/\gamma < 1$ fm, they play an important role in the collision dynamics.

As a result of the collision of two nuclei, or rather two clouds of wee partons, a highly excited matter with a large number of virtual quanta is created in the mid-rapidity region. (In the modern parlance one talks about coherent "glasma" formed by a collision of two sheets of "colour glass condensates (CGC)" [35].) Hereinafter we discuss only the mid-rapidity region. The virtual quanta need a finite time (τ_{dec}) to decohere and turn into real quarks and gluons. Here τ_{dec} refers to the rest frame of an individual parton. In the overall CM frame, the relevant time is $\gamma\tau_{dec}$ due to the time dilation, γ being the Lorentz factor of the parton. It is now clear that "slow" partons decohere earlier and hence near the origin, than the "fast" ones which emerge later at points farther away from the origin. (This is known as the inside-outside cascade.) In other words, the large-x part of each nuclear wave function continues to move along its light-cone trajectory leaving the small-x part behind. Thus, in the limit of high beam energy, the time dilation effect causes the near transparency of nuclei, referred to earlier.

Figure 12 shows this schematically in 1+1 dimension for simplicity. The curves are hyperbolas of constant proper time $\tau = \sqrt{t^2 - z^2}$. All points on a given hyperbola are at the same stage of evolution. In particular, let the hyperbola labelled '1' refer to $\tau = \tau_{dec}$. Parton at z undergoes decoherence at time $t = \sqrt{\tau^2_{dec} + z^2}$. The larger the z, the larger the time t and higher the parton velocity $v_z = z/t$ [34].

If the partons thus formed interact amongst themselves a multiple number of times, the system approaches local thermal equilibrium. Thermalization time τ_{th} ($> \tau_{dec}$) is estimated to be of the order of 1 fm.

Figure 12 indicates a possible scenario. $1;\ldots;5$ are the hyperbolas with proper times $\tau_1;\ldots;\tau_5$.

$t = 0 = z$: the instant of collision

$0 < \tau < \tau_1$: formation of quark-gluon matter

$\tau_1 < \tau < \tau_2$: (local) equilibration of quark-gluon matter, i.e., formation of QGP
$\tau_2 < \tau < \tau_3$: hydrodynamic evolution of QGP (partonic EOS)
$\tau = \tau_3$: hadronization
$\tau_3 < \tau < \tau_4$: hydrodynamic evolution (hadronic EOS)
$\tau_4 < \tau < \tau_5$: transport theoretic evolution of hadrons
$\tau = \tau_5$: freezeout
$\tau > \tau_5$: free-streaming to detectors

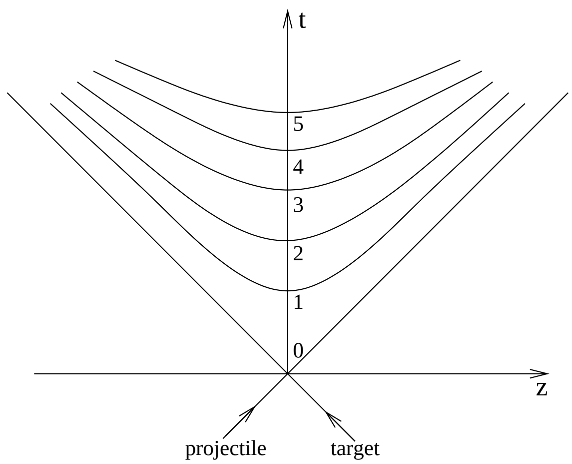

Figure 12. Space-time picture of an ultra-relativistic nucleus-nucleus collision in 1 + 1 D for simplicity

The above is a rather simple-minded picture: in reality, there are no such "water-tight compartments". The framework of hydrodynamics is applicable, if at all, only when the system is at or near (local) thermal equilibrium. If the matter formed in ultrarelativistic heavy-ion collisions is fully thermalized, one may use the framework of relativistic ideal fluid dynamics to study its evolution. If it is only partially thermalized, one could use relativistic dissipative fluid dynamics. In any case, the covariant transport theory provides a more general framework for this purpose.

Bjorken [34] presented the following formula to estimate the energy density attained in the mid-rapidity region:

$$\varepsilon_0 = \frac{1}{\pi R^2 \tau_f} \frac{dE_T}{dy}\bigg|_{y=0}, \qquad (4)$$

where R is the nuclear radius, $\tau_f \sim 1$ fm/c is the formation time of QGP, and E_T is the transverse energy.

It is clear that even if QGP is formed, its lifetime will be of the order of a few fm/c or $O(10^{-23})$ seconds, and what experimentalists detect in their detectors are not quarks or gluons, but the standard hadrons, leptons, photons, etc. It is a highly nontrivial task to deduce the formation of QGP from the properties of the detected particles. This is analogous to the situation in cosmology where one tries to deduce the information on the early epochs after the Big Bang by studying the cosmic microwave background radiation and its anisotropy.

Actually the analogy between the Big Bang and the "Little Bang" is quite striking. In both the cases the initial conditions are not accurately known, but there are plausible scenarios. In the former case, there is inflation occurring at $\sim 10^{-35}$ sec, with the inflaton energy converting into matter and radiation, leading to a thermal era. In the latter case, one talks about a highly excited but coherent glasma converting, on the time scale of $\sim 10^{-24}$ sec, into quarks and gluons which may thermalize to form QGP. In both the cases the "fireball" expands, cools, and undergoes one or more (phase) transitions. Decoupling or freezeout follows — of photons in the former case and of hadrons in the latter. The unknown initial conditions are parameterized and one tries to learn about them by working one's way backwards, starting with the detected particles. As we shall see shortly, the anisotropy of the detected particles plays a crucial role in the diagnostics of the Little Bang too.

Definition: The STAR collaboration at RHIC has defined the QGP as "a (locally) thermally equilibrated state of matter in which quarks and gluons are deconfined from hadrons, so that colour degrees of freedom become manifest over nuclear, rather than merely nucleonic, volumes" [36]. The two essential ingredients of this definition are (a) local equilibration of matter, and (b) deconfinement of colour over nuclear volumes. Recent claims of the discovery of QGP at RHIC [37] were based on two observations which, for the first time, provided a good evidence that each of these two requirements has been fulfilled. We discuss them one by one in the next two subsections (3.2, 3.3). That will be followed by brief descriptions of a few other signals of QGP in subsections 3.4, 3.5.

3.2. Anisotropic Flow

Consider now a non-central (or non-zero impact parameter) collision of two identical (spherical) nuclei travelling in opposite directions. Choose x, y axes as shown in Fig. 13. The collision or beam axis is perpendicular to the plane of the figure. Length of the line AB connecting the centres of the two nuclei is the impact parameter b. Plane xy is the azimuthal or transverse plane. Plane xz is the reaction plane. It is determined by the impact parameter vector b and the collision axis. (Obviously the reaction plane cannot be defined for a central collision.) $\phi = \tan^{-1}(p_y/p_x)$ is the azimuthal angle of an outgoing particle. The almond-shaped shaded area is the overlap zone. In a real experiment, Fig. 14, the x, y axes need not coincide with the lab-fixed X, Y axes. Indeed the reaction plane subtends an arbitrary angle ϕ_R with the X axis. ϕ_R varies from event to event. It is a priori unknown and special experimental techniques are needed for its determination.

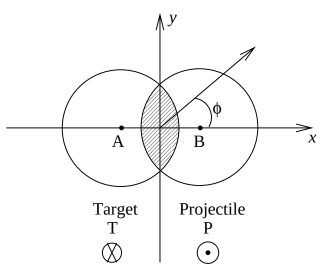

Figure 13. Non-central collision

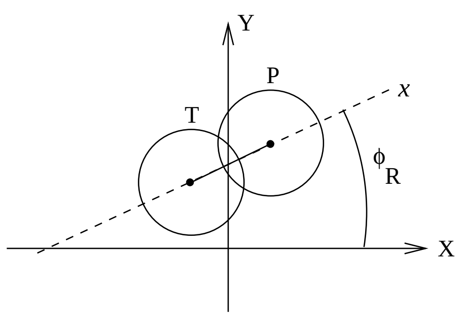

Figure 14. Non-central collision. XY are lab-fixed axes.

The triple differential invariant distribution of particles emitted in the final state of a heavy-ion collision is a periodic even function of ϕ, and can be Fourier decomposed as

$$E\frac{d^3N}{d^3p} = \frac{d^3N}{p_T\,dp_T\,dy\,d\phi} = \frac{d^2N}{p_T\,dp_T\,dy}\frac{1}{2\pi}\left[1+\sum_{1}^{\infty}2v_n\cos(n\phi)\right];$$

where y is the rapidity and ϕ is measured with respect to the reaction plane. The leading term in the square brackets in the above expression represents the azimuthally symmetric radial flow. v_1 is called the directed flow and v_2 the elliptic flow. $v_n \equiv \langle\cos(n\phi)\rangle$ is actually a function of p_T and y. Here the average is taken with a weight equal to the triple differential distribution of particles in the (p_T, y) bin under consideration. v_2 can also be written as $\langle(p_x^2 - p_y^2)/(p_x^2 + p_y^2)\rangle$. For a central collision the distribution is azimuthally isotropic and hence $v_n = 0$ for $n = 1, 2, ...$ In other words, only the radial flow survives.

Measurement of the radial flow: Radial flow gives a radially outward kick to the emerging hadrons thereby depleting the low-p_T population and making their p_T spectra flatter. The heavier the hadron, the stronger the momentum kick it receives. By measuring the slopes of the p_T spectra of various hadrons, the radial flow velocity can be extracted. At RHIC it turns out to be a sizeable fraction ($\sim 50\%$) of the speed of light. Thus the flow is compressible.

Measurement of the anisotropic flow v_n: There are several methods. (a) The most obvious one is based on the definition $v_n \equiv \langle\cos n(\phi - \phi_R)\rangle$ where both ϕ and ϕ_R are measured with respect to a lab-fixed frame of reference. This, however, requires the knowledge of ϕ_R which varies from event to event and is not easy to determine. (b) Two-particle correlation method: This gives $v_n^2 = \langle\cos n(\phi_1 - \phi_2)\rangle$, where ϕ_1 and ϕ_2 are azimuthal angles of two outgoing particles. This method has an advantage that the reaction plane need not be known. However, v_n is determined only up to the sign. There are several other methods such as the cumulant method [38], mixed-harmonic method [39], Lee-Yang zeroes method [40], etc. For a recent review, see [41].

Importance of the anisotropic flow v_n: Consider a non-central collision, Fig. 13. Thus the initial state is characterized by a spatial anisotropy in the azimuthal plane. Consider particles in the almond-shaped overlap zone. Their initial momenta are predominantly longitudinal. Transverse momenta, if any, are distributed isotropically. Hence $v_n(\text{initial}) = 0$. Now if these particles do not interact with each other, the final (azimuthal) distribution too will be isotropic. Hence $v_n(\text{final}) = 0$.

On the other hand, if these particles interact with each other a multiple number of times, then the (local) thermal equilibrium is likely to be reached. Once that happens, the system can be described in terms of thermodynamic quantities such as temperature, pressure, etc. The spatial anisotropy of the almond-shaped overlap zone ensures anisotropic pressure gradients in the transverse plane. This leads to a final state characterized by a momentum anisotropy in the $p_x p_y$ plane or equivalently[1] to an anisotropic distribution of particles in the transverse (xy) plane, and hence a nonvanishing v_n. Thus v_n is a measure of the degree of thermalization of the matter produced in a noncentral heavy-ion collision.

To sum up, if either of the two ingredients, namely initial spatial anisotropy and adequate rescatterings, is missing, there is no anisotropic flow (v_n).

Sensitivity of v_n to properties of matter at early times (fm/c): We saw above that the spatial anisotropy of the initial state (together with multiple rescatterings) leads to more matter being transported in the directions of the steepest pressure gradients, and thus to a non-zero v_n. That in turn results in the reduction in spatial anisotropy ("self-quenching"). In other words, expansion of the source gradually diminishes its spatial anisotropy. Thus v_n builds up early (i.e., when the spatial anisotropy is significant) and tends to saturate as the spatial anisotropy continues to decrease. (This is unlike the radial flow which continues to grow until freeze-out and is sensitive to early- as well as late-time history of the matter). Thus v_n is a measure of the degree of thermalization of the matter produced early in the collision. In other words, v_n is a signature of pressure at early times.

Hydrodynamic calculations of v_n involve the equation of state of QGP. Thus one hopes to learn about the material properties of the medium, such as the speed of sound, sheer and bulk viscosities, relaxation times, etc.

Flow may also be affected by the dynamics of the hadronic phase. Study of the flow would provide constraints on the properties of hadronic matter too. (It is expected that at LHC, the relative contribution of the QGP phase to v_n would be larger than that at SPS and RHIC. This would reduce the effect of the uncertainties in the hadronic phase).

It should, however, be kept in mind that the initial conditions for the hydrodynamic evolution are not known with certainty. Hence the task of unravelling the properties of medium is not as easy as it may appear.

Figure 15 shows the impressive agreement between RHIC data on $v_2(p_T)$ and ideal hydro calculations for p_T up to 1.5 GeV/c. In particular note the mass ordering: the heavier the hadron, the smaller the $v_2(p_T)$. This can be understood heuristically as follows.

Mass ordering of $v_2(p_T)$: Recall that the radial flow depletes the population of low-p_T hadrons (by shifting them to larger values of p_T). This effect is more pronounced for larger flow velocities and for heavier hadrons. Suppose v_2 is positive as at RHIC, which means more hadrons emerge in-plane (x-direction) than out-of-plane (y-direction). Now due to higher pressure gradients in the x-direction, hadrons which emerge in-plane experience a larger flow velocity than those which emerge out-of-plane. So the depletion is greater for the hadrons emerging in-plane than out-of-plane. This tends to reduce the anisotropy and hence v_2 of all hadron species. For a heavier hadron species this reduction is more pronounced. The net result is $v_2^{\text{light hadron}}(p_T) > v_2^{\text{heavy hadron}}(p_T)$. Mass-ordering signifies a common radial velocity field.

Hydrodynamic model calculations predicted mass ordering of $v_2(p_T)$. The broad agreement between the RHIC data and the predictions of ideal hydro (Fig. 15) led to the claims of thermalization of matter and discovery of a perfect fluid — more perfect than any seen before.

In order to claim the discovery of a new state of matter, namely quark-gluon plasma, one needs to demonstrate unambiguously that (local) equilibrium is attained. There are indications that the equilibrium attained at RHIC is incomplete [42].

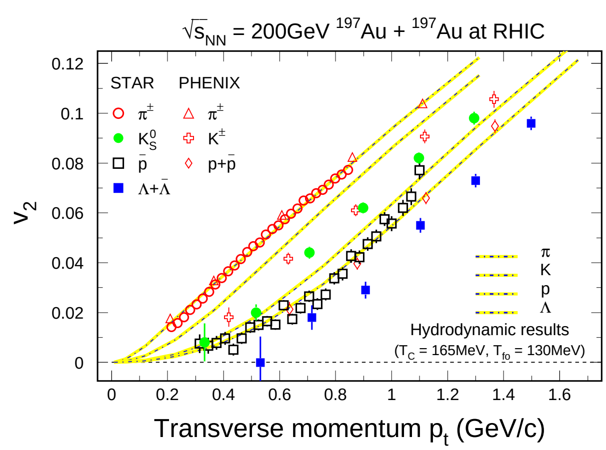

Figure 15. Minimum-bias data. Curves represent ideal hydro results with a first-order QGP-hadron phase transition. Figure taken from [43].

[1] Since $= \tan^{-1}(p_y/p_x)$.

3.2.1. Constituent Quark Scaling

For $p_T > 2$ GeV/c, ideal hydro results are in gross disagreement with the $v_2(p_T)$ data: calculated $v_2(p_T)$ continues to rise with p_T, while the data tend to saturate and the mass ordering is reversed. In the intermediate momentum range (2 GeV/c $< p_T <$ 5 GeV/c), it is observed that the v_2/n_q vs p_T/n_q (or KE_T/n_q) data fall on a nearly universal curve; see Fig. 16. Here n_q is the number of constituent quarks and KE_T is the transverse kinetic energy. This is called the constituent quark scaling. It shows that the flow is developed at the quark level, and that the hadronization occurs by quark recombination.

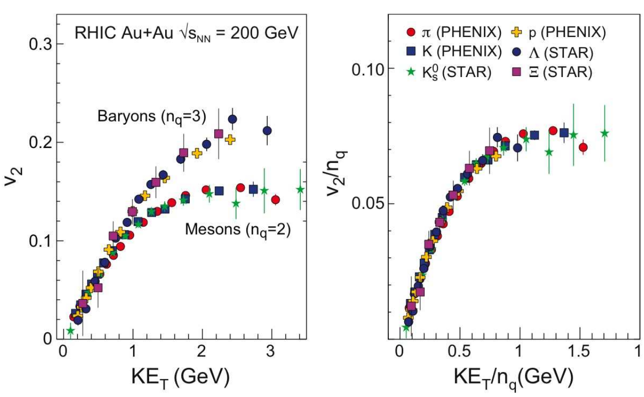

Figure 16. Left: Note the two distinct branches. Right: Universal curve. Figure taken from [44].

3.3. Jet Quenching

A variety of signatures of quark-gluon plasma have been proposed. Some of the more popular ones are excess strangeness production, thermal dileptons and photons, jet quenching, J/ψ-suppression and event-by-event fluctuations. A common theme underlying all of these is the idea of exploiting the consequences of those properties of QGP which distinguish it from alternatives like a hot hadron gas. Since QGP is expected to form and exist predominantly in the early phase of the collision, the so-called hard probes are potentially the cleaner direct probes of this early phase. It is experimentally known that rare but highly energetic scatterings produce jets of particles: $g + g \to g + g$, where energetic gluons from the colliding hadrons produce two gluons at large transverse momenta, which fragment and emerge as jets of showering particles. Their typical production time scale is $t \sim 1/Q$, where $Q = p_T$, the transverse momentum of the jet, is the hard scale of production. Thus jets at large transverse momenta are produced very early and by traversing through the produced medium carry its memory while emerging out. Quark-Gluon Plasma, or any medium in general, interacts with the jet, causing it to lose energy. This phenomenon goes by the name of jet quenching.

Using the well-known factorization property of perturbative QCD [45], which allows a separation between the hard and soft scales, a typical cross section at hard scale, say that of hadron h at large transverse momenta in the process $A + B \to h + X$, can be symbolically written as

$$\sigma_{AB\to h} = f_A(x_1;Q^2) \otimes f_B(x_2;Q^2) \otimes \sigma(x_1;x_2;Q^2) \otimes D_{i\to h}(z;Q^2) . \quad (5)$$

Here f_A, f_B are parton distribution functions of the colliding hadrons A and B at scale Q^2, $\sigma(x_1;x_2;Q^2)$ is the elementary pQCD cross section for partons of momentum fractions x_1 and x_2 to produce a parton i with the hard scale $Q = p_T$ for jet production, and $D_{i\to h}(z;Q^2)$ is its fragmentation function to hadron h with momentum fraction z. Various convolution integrations are denoted symbolically by $\otimes$. Clearly, there are many more details which are not spelt out here for brevity, such as the kinematic integration region or the summation over all allowed many parton level processes, such quark-quark or gluon-quark etc. These can be found in textbooks [45].

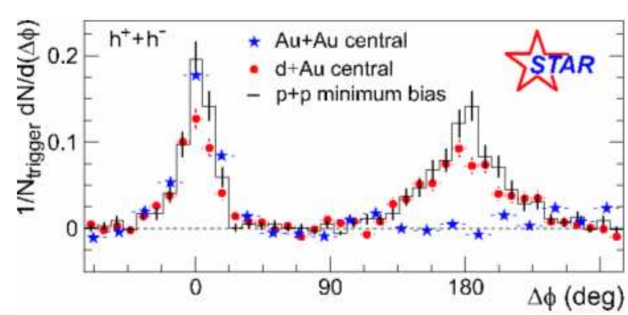

Figure 17. Comparison of the various dihadron angular correlations. Taken from [47].

In presence of a medium, of hot hadron gas or quark-gluon plasma, the function D above will get modified by the interactions with medium. The medium provides scattering centers for the fast moving seed particle of the jet which typically impart a transverse momentum kick to it. The medium induced transverse momentum squared per unit path length, $\hat{q}$, characterizes

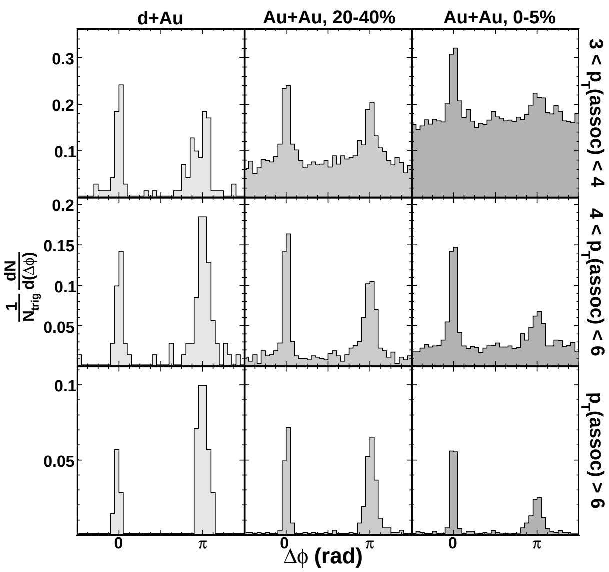

Figure 18. Comparison of the dihadron azimuthal correlations as a function of the associated p_T for 8 < p_T^{trigg} < 15 GeV. Taken from [48].

the quenching weight function $P(\Delta E)$ [46] which is the probability that a hard parton loses an additional energy ΔE due to its interactions with the medium. In hot matter with a temperature of about T = 250 MeV, a perturbative estimate [49] for $\hat{q}$ is about 0.5 GeV^2/fm. It is typically a lot smaller in the cold nuclear matter. In terms of the quenching weight, one can write down [46] a medium modified fragmentation function for a jet passing through a medium as

$$D^{med}_{i\to h}(x;Q^2) = \int_0^1 d\epsilon \, \frac{P_E(\epsilon)}{1-\epsilon} D_{i\to h}\left(\frac{x}{1-\epsilon};Q^2\right) . \qquad (6)$$

For a heavy quarkonium like J/ψ, the analogue of D, is the wave function of a heavy quark-antiquark pair ($c\bar{c}$), and it will be presumably flatter in a hot medium, corresponding to "its melting".

RHIC experiments have cleverly exploited their capabilities to perform tests which have an on-off nature and are therefore rather convincing about the qualitative existence of the jet quenching phenomenon in heavy ion collisions. In the case of the elementary $g + g \to g + g$ hard process, one expects back-to-back jets, i.e, a well-determined azimuthal correlation between the fast particles. As jets are hard to identify in the complex multi-particle environment at RHIC, the STAR collaboration constructed the angular correlation of hadrons, using a high transverse momentum p_T^{trigg} particle as the trigger, and studying the azimuthal distributions of the associated particles ($p_T^{assoc} < p_T^{trigg}$). Figure 17 compares the results for gold-gold central collisions, where one expects formation of a hot medium, with the proton-proton or deuterium-gold collisions, where one expects to have turned off the medium effects. The expected correlation, signalling a lack of any quenching/medium, is clearly visible in the two peaks separated by 180° for the d-Au and pp collisions. Remarkably the gold-gold central collision data show only the peak at zero degree or the near-side. A hint of the creation of some medium is given by the vanishing of the away-side jet, at 180 degrees, which appears to have been fully quenched by the medium. For high enough trigger p_T, one can do the same comparison as a function of range of the associated p_T. Clearly, as the p_T^{assoc} increases, one ought to see the away-side re-emerge. This is beautifully seen in the Figure 18. It shows the azimuthal correlations for 8 < p_T^{trigg} < 15 GeV for d-Au, and Au-Au collisions in two centrality bins, with the data for most central collisions displayed in the last column. The p_T of the associated particle is restricted to ranges marked on the right side, and increases as one goes from top to the bottom. All panels show comparable strengths for the near-side peak. As the p_T^{assoc} grows above 6 GeV, the away-side peaks in all the three systems also show comparable strengths whereas for lower p_T^{assoc} ranges one has diminishing away-side peaks, characteristic of jet-quenching. The same phenomena can also be studied by varying the p_T^{trigg} and the away-side peak is seen clearly to emerge as p_T^{trigg} increases.

A more quantitative investigation of the jet quenching phenomena needs to extract the transport coefficient $\hat{q}$, and establish the presence of the hot matter by comparing it with the corresponding theoretical estimates, directly from QCD. Many such attempts have been made. Recently, the PHENIX experiment [51] reported their measurement of neutral pion production in Au-Au collisions at 200 GeV at the RHIC collider in BNL. They define the now-famous nuclear suppression factor R_{AA} as the weighted ratio of the nuclear differential distribution in rapidity y and transverse momentum p_T and their own earlier measurements for the same quantity in proton-proton,

$$R_{AA} = \frac{1/N_{evt}\, dN/dy dp_T}{\langle T_{AB}\rangle \, d\sigma_{pp}/dy dp_T} \; , \qquad (7)$$

where further details of determinations of various factors above are given in [51]. Their results for R_{AA} are displayed in Figure 19. While the first panel shows the results for their entire data set, the other panels exhibit

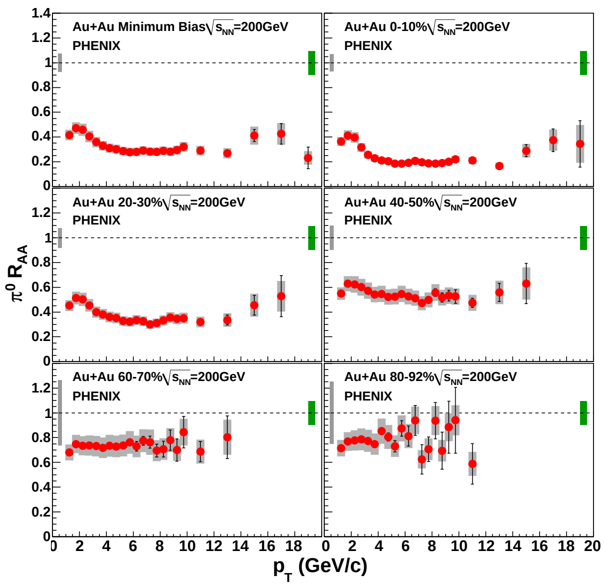

Figure 19. Nuclear modification factor, R_{AA}, for neutral pions as a function of transverse momentum for different centralities. Taken from [51].

data for increasing peripherality of the collisions (indicated by the increasing range of the percentage label of each panel), or decreasing centrality. The error bars indicate the statistical errors, whereas various systematic errors are shown by the boxes. Note that if the nucleus-nucleus collisions were merely scaled proton-proton ones, one expects R_{AA} = 1. What the data in Figure 19 indicate, however, is a five-fold suppression that is essentially constant for $5 < p_T < 20$ GeV for the most central bin of 0-10 %. The qualitative pattern is the same in all centralities, although the magnitude of suppression comes down. The highest centrality bin was used to determine the transport coefficient in the parton quenching model [50] to obtain $\hat{q} = 13.2^{+2.1}_{-3.2}$ GeV^2/fm. Typically, fits with varying model assumptions do tend to yield a $\hat{q}$ of 5-15 GeV^2/fm. This order of magnitude or so higher value of the transport coefficient compared to the expectations from perturbative QCD, ~ 0.5, as mentioned above is an unresolved puzzle. Nevertheless, the value hints at a hot medium, presumably even stronger interacting than the pQCD picture, as the cold matter expectations for $\hat{q}$ are even more in disagreement with the experimental determination. Clearly a lot more needs to be understood from the data by further delving into the detail predictions of the models and confronting them with data, as [51] attempts to do, in order to establish the nature of hot medium produced as that of quark-gluon plasma.

Having discussed the two main observations, anisotropic flow and jet quenching, which lend support to the claims of discovery of QGP at RHIC, we now discuss some corroborative evidences which strengthen these claims. There are also surprises in the RHIC data when compared with the expectations from the earlier lower energy heavy ion collisions at SPS in CERN. We discuss some with the aim to prepare ourselves for the expectation at yet higher energy in LHC.

3.4. Anomalous J/ψ Suppression

Amongst the many signatures proposed to look for QGP experimentally, the idea of J/ψ-suppression has attracted the most attention as the likely "gold-plated" signal. Soon after the pioneering work of Matsui and Satz [23], arguing that i) as a hard QCD process, the heavy charm pair production takes place very early, ii) the Debye screening of the QGP prevents formation of a J/ψ state in heavy ion collisions, and iii) the low temperatures at the hadronization do not permit production of charm-anticharm pair kinematically, it was further proposed that the suppression pattern ought to have a characteristic [52] transverse momentum dependence. Recognising that the gluon and quark distribution functions depend on the atomic number A, known by the famous EMC-effect, it was shown in a perturbative QCD calculation that the suppression signal [53] itself as well as its p_T-dependence [54] can be mimicked by the mundane nuclear shadowing. Thus it became clear since the early days that a detailed quantitative analysis is necessary to disentangle the effects of the Debye screening in QGP. It has since been recognised that other effects, notably the absorption [55] of the produced J/ψ in the nucleus, causes suppression of J/ψ in all pA and AB-collisions. Thus one has to first account for this expected or normal suppression and then look for additional or anomalous J/ψ-suppression as the possible signal of QGP. Considering the general wisdom that J/ψ-production can be computed in pQCD, it ought to be a straightforward task to compute this normal suppression. Unfortunately, it is not so. One reason is that the gluon distribution function, and the nuclear shadowing effects, are not well known. Another, perhaps much more important reason, is that the hadroproduction of J/ψ needs to tackle the vexing issue of its formation from the perturbatively produced charm-anticharm pair. One usually depends [56] on models, such as the colour evaporation or the color octet model, hoping that the effective theory descriptions are valid. It turns out to be true for large p_T charmonium production but not for the total cross sections of interest for the QGP signal.

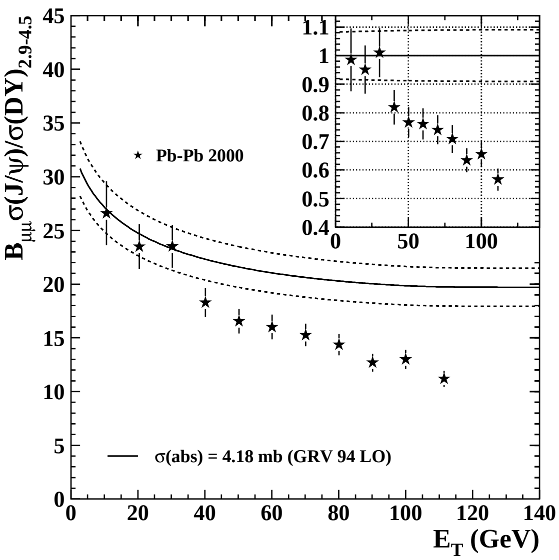

Figure 20. J/ψ-suppression in Pb-Pb collisions at SPS as a function of transverse energy E_T. Figure taken from [57].

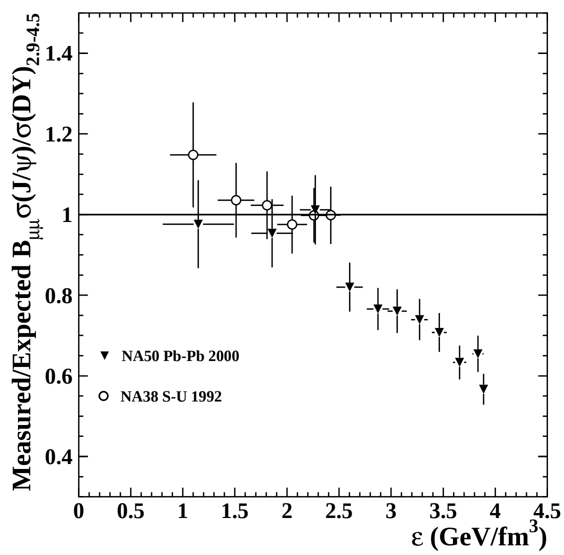

Figure 21. J/ψ-suppression in Pb-Pb collisions at SPS as a function of the energy density ϵ. Figure taken from [57].

The preferred phenomenological method [55] has been to parametrise the ratio of J/ψ-cross sections, total or appropriate differential cross sections in its transverse momentum p_T, or forward momentum fraction x_F etc., in pA and pp collisions at the same colliding energy, $\sqrt{s}$, as $\exp(-\sigma_{abs}(J/\psi)\rho_0 L)$, where L is the mean length of the trajectory of the produced $c\bar{c}$ pair in nuclear matter and ρ_0 is the nuclear density. The parameter, $\sigma_{abs}(J/\psi)$, is obtained by fitting the data. Defining a mean free path $\lambda = 1/\sigma_{abs}(J/\psi)\rho_0$, one then extends this idea to the heavy-ion collisions to define the normal or expected J/ψ suppression due to the traversing of the $c\bar{c}$-pair in the nuclear matter as $\exp(-(L_A + L_B)/\lambda)$. Here L_A and L_B are the lengths for the trajectories of the $c\bar{c}$ in the projectile (A) and target (B) respectively. They are calculated from collision geometry by using the oft-used relations between mean transverse energy of the bin, E_T, and the average impact parameter b.

Figure 20 exhibits [57] the results of the NA50 collaboration on J/ψ cross section as a function of the transverse energy E_T in Pb-Pb collisions at $\sqrt{s} \simeq 17$ GeV. It is normalized to the Drell-Yan cross section in the mass range shown and $B_{\mu\mu}$ is the branching fraction of J/ψ in the dimuon channel. The full curve depicts the expected normal suppression as a function of E_T, computed as explained above using the fitted J/ψ cross section of 4.18 mb obtained from the NA50's own pA data. The dashed lines show the computed error bars on the expected suppression, and the inset shows the ratio of measured to the expected suppression. Using the Bjorken formula in eq. (4), one obtains this ratio of the measured to the expected cross section ratio of the J/ψ and the Drell-Yan as a function of the energy density in GeV/fm^3 units, as shown in Figure 21, taken from [57]. One sees that the anomalous suppression, i.e., depletion of the measured cross section from that expected, sets in at an energy density of about 2.5 GeV/fm^3, comparable to the expectations from lattice QCD, as seen in Figure 4. A natural explanation of the anomalous suppression was, therefore, the formation of quark-gluon plasma. Since the J/ψ-production takes place both directly and through other charmonium states like χ_c, the slow fall-off with the energy density in Figure 21 could be interpreted as gradual progress towards the full suppression. However, one could also explain the anomalous suppression in alternative ways, using hadronic [58] or thermal [59] models. Since one expects the higher collision energy at RHIC to produce higher temperatures/energy densities, one expected a further stronger suppression at RHIC. Indeed, this seems to be true both in the quark-gluon plasma models as well as the alternatives, the difference between them being quantitative in nature.

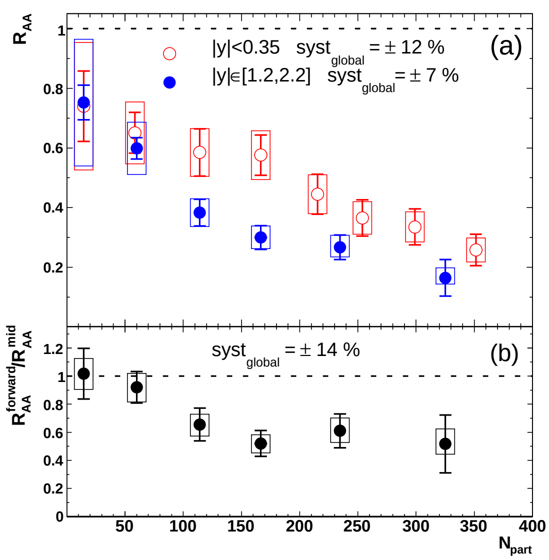

Figure 22. J/ψ-suppression in Au-Au collisions at PHENIX, BNL as a function of number of participants. Figure taken from [60].

The RHIC results [60], however, brought a big surprise by being different from any of those expectations. Analogous to the case of jet quenching in the previous section, the PHENIX collaboration at RHIC constructs the ratio R_{AA} of the J/ψ (differential) production cross section in AA collisions and the corresponding pp cross section weighted by the number of binary collisions. Figure 22 displays their results for R_{AA} in Au-Au collisions at $\sqrt{s} = 200$ GeV. They show more suppression in the forward region ($|y| \in [1.2, 2.2]$, filled circles in the top panel), than the central ($|y| < 0.35$, open circles in the top panel) for number of participants greater than 100 (alternatively for large enough transverse energy E_T). More importantly, a direct comparison [61] in Figure 23 clearly demonstrates that the PHENIX data in the central rapidity region are in very good agreement with the CERN NA50 results [57]. The trends for both the central region of the CERN and RHIC experiments, as seen in Figure 23, and the ratio of forward to the central rapidity region, as seen in the bottom panel of Figure 22, are against [61] the predictions of the models which successfully accounted for the NA50 data.

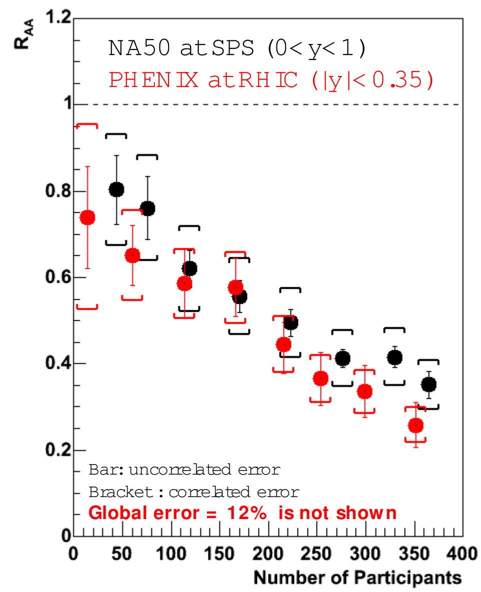

Figure 23. Comparison of NA50 and PHENIX results on J/ψ-suppression as a function of number of participants. Figure taken from [61].

There have been some attempts to solve this J/ψ-puzzle. As we saw in the Figure 10 of section 2.4, the lattice QCD results suggest melting of the J/ψ takes place at higher temperatures ($> 2T_c$) than predicted by simple models. A way to understand the results in Figure 23 could then suggest itself if the temperature reached at both the SPS and RHIC energy is $< 2T_c$. In that case, only χ_c and ψ^0 would have melted [62], suppressing the corresponding decay J/ψ's, and giving similar results for CERN and RHIC experiments. Since the temperature reached at LHC is expected to cross $2T_c$, a clear prediction of such a scenario would then be much more suppression for LHC than that in Figure 23. However, there are other scenarios, including thermal enhancement [63] arising due to recombination of the large number of thermal produced charm-anticharm quarks. These would predict an overall enhancement. In any case, J/ψ-suppression could provide a lot of excitement again at LHC.

3.5. Particle ratios & Bulk Properties

A variety of hadrons are produced in an ultra-relativistic heavy-ion collision. They are identified and their relative yields measured; see Fig. 24. These hadron abundance ratios can be calculated in a simple statistical model [64]: It is assumed that these particles emerge from a chemically equilibrated hadron gas characterized by a chemical potential (μ_i) for each hadron species and a common temperature (T). The number density n_i of hadron of type i is then given by the standard Fermi-Dirac (+) or Bose-Einstein ($-$) formulas

$$n_i = d_i \int \frac{d^3p}{(2\pi)^3} \frac{1}{\exp[(E_i - \mu_i)/T] \mp 1},$$

where d_i is the spin degeneracy. At chemical equilibrium, the chemical potential μ_i can be written as $\mu_i = \mu_B B_i - \mu_S S_i - \mu_I I_i^{(3)}$ where B_i, S_i and $I_i^{(3)}$ stand for the baryon number, the strangeness and the third component of the isospin quantum numbers, respectively, of the hadron of type i. The two unknown parameters T and μ_B are fitted to the data. This simple model has been quite successful in explaining the SPS and RHIC data; see Fig. 24 for SPS and a similar figure in [65] for RHIC. Note that even the multistrange particles seem to be consistent with the model. This suggests that they are produced in a partonic environment rather than in a hadronic one. $T \approx T_{ch}$ is the chemical freezeout temperature. The fitted values are

$$T_{ch} = 170\ \mathrm{MeV}, \quad \mu_B = 270\ \mathrm{MeV}, \ (\mathrm{SPS});$$
$$T_{ch} = 176\ \mathrm{MeV}, \quad \mu_B = 41\ \mathrm{MeV}, \ (\mathrm{RHIC}\ 130\ \mathrm{GeV});$$
$$T_{ch} = 177\ \mathrm{MeV}, \quad \mu_B = 29\ \mathrm{MeV}, \ (\mathrm{RHIC}\ 200\ \mathrm{GeV}).$$

Note the trend of the chemical freezeout point to approach the temperature axis of the QCD phase diagram as the collision energy is increased. Data obtained at the AGS and SIS energies are also consistent with this trend; see Fig. 1.3 in [66]. For more recent fits to the statistical model, see [67].

4. Hydrodynamics

Hydro plays a central role in modelling relativistic heavy-ion collisions: It is first used for the calculation of the p_T spectra and the elliptic flow v_2. The resultant energy density or temperature profiles are then used in the calculations of jet quenching, J/ψ melting, thermal photon and dilepton production, etc.

Hydrodynamic framework consists of a set of coupled partial differential equations for energy density, number density, pressure, hydrodynamic four-velocity, etc. In addition, these equations also contain various transport coefficients and relaxation times.

Hydro is a very powerful technique because given the initial conditions and the EOS it predicts the evolution of the matter. Its limitation is that it is applicable at or near (local) thermodynamic equilibrium only.

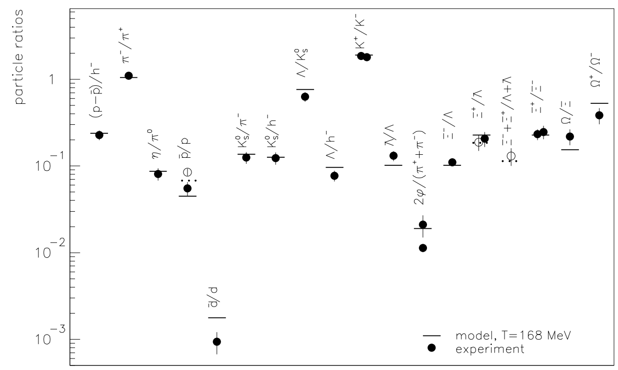

Figure 24. Comparison between the statistical model (horizontal bars) and experimental particle ratios (filled circles) measured at SPS CERN. From Braun-Munzinger et al. [64].

4.1. A Perfect Fluid?

How robust is the claim of discovery of a perfect fluid at RHIC, or is there any need of the viscous hydrodynamics for RHIC? A closer scrutiny shows that the claim is not really robust, and it is necessary to do viscous hydro calculations:

Agreement between data and ideal hydro is far from perfect. (Ideal) "hydro models seem to work for minimum-bias data but not for centrality-selected and p data" [68].

Initial (and final) conditions for the hydrodynamic regime are uncertain. It is entirely possible that the ideal hydro mimics viscous hydro if the initial (and/or final) conditions are suitably tuned. Most ideal hydro calculations so far have been done with Glauber-type initial conditions. It has recently been realized that the CGC-type initial conditions yield higher eccentricity of the overlap zone [69], and hence higher v_2. To push these results down to agree with data, some viscous corrections are needed. The same is true with fluctuations in the initial conditions [70]. Event-to-event fluctuations in nucleon positions result in higher eccentricity and hence higher v_2 [71].

Some v_2 may build up during the pre-equilibrium (i.e., pre-hydro) regime. Success of ideal hydro may be due to the neglect of this contribution to v_2 in most calculations [72].

For realistic light quark masses, the deconfinement transition is known to be a smooth crossover. However, it seems that the ideal hydro calculations need a first-order transition for a best fit to the data [73].

The shear viscosity to entropy density ratio (η/s) may be small in the transition region. But there are indications that the bulk viscosity to entropy density ratio (ζ/s) may be rising dramatically near T_c [74]. If this result holds, QGP discovered at RHIC cannot be called a perfect fluid.

It is known that for helium, water, nitrogen, η/s at constant pressure plotted as a function of temperature, exhibits a minimum with a cusp-like behaviour at the critical point; see Fig. 25. There are indications that the QCD matter too shows similar trends. Viscous hydro calculations of the QCD matter would allow us to extract η/s from data and might help us pinpoint the location of the QCD critical point [75].

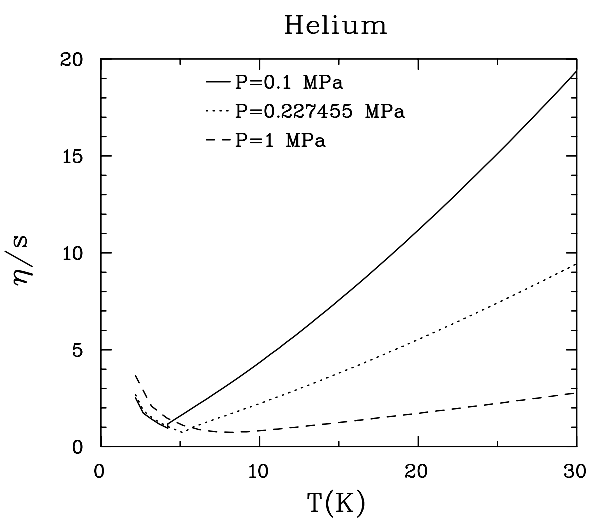

Figure 25. Each curve is at a fixed pressure. Solid: below the critical pressure P_c, dotted: at P_c, dashed: above P_c. From [75].

If the inequality $\eta/s \geq 1/4\pi$ obtained [16] from the AdS/CFT duality is applicable to QCD, then also viscous hydro calculations become necessary.

Assume a quasiparticle picture. Quantum mechanical uncertainty principle tells us that the mean-free path (λ) cannot be less than the inverse of the typical momentum of the quanta. It also makes no sense to have a mean-free path smaller than the interparticle spacing [76]. Since $\eta \propto \lambda$, η cannot vanish.

Finally, to claim success for ideal hydro, one should calculate viscous corrections and show explicitly that they are indeed small.

4.2. Relativistic Dissipative Hydro — a Brief History

Relativistic version of the Navier-Stokes equation was obtained by Eckart [77], and by Landau and Lifshitz [78]. This is called the standard or the first-order formalism because terms only up to first order in dissipative quantities are retained in the entropy four-current. (The Euler's equation constitutes the zeroth-order formalism.) However, it was soon realized that this formalism suffers from the following problems:

- Acausality: Equations are parabolic and they result in super-luminal propagation of signals [79, 80].
- Instability: Equilibrium states are unstable under small perturbations for a moving fluid [81]. This makes it difficult to perform controlled numerical simulations.
- Lack of relativistic covariance: This problem is related to the previous one. First-order theories look covariant, but they are not.

A causal dissipative formalism was developed by Muller [79], and Israel and Stewart [80], in the non-relativistic and relativistic sectors, respectively. It is also called a second-order formalism because the entropy four-current now contains terms up to second order in dissipative quantities. The resulting hydrodynamic equations are hyperbolic. Application of causal dissipative hydro to relativistic heavy-ion collisions was pioneered by Muronga [82]. Since then many others have contributed to this effort. We shall describe some of them in subsection 4.4.

Recent years have witnessed intense activity in the area of causal hydro of gauge theory plasmas from AdS/CFT duality; for reviews see [83].

4.3. Basic Idea of Causal Dissipative Hydro

Before we discuss hydrodynamics, let us first consider a simpler example of diffusion. Consider a fluid in equilibrium with a uniform density ρ. If the fluid is perturbed such that the density is no longer uniform, it responds by setting up currents which tend to restore the equilibrium. In the linear response theory, the induced current J_i is simply proportional to the gradient of ρ (Fick's law):

$$J_i = -D\,\partial_i \rho\,, \tag{8}$$

where D is the diffusion coefficient. D is an example of a transport coefficient. Transport coefficients play an important role in the study of relaxation phenomena in non-equilibrium statistical mechanics or fluid dynamics. Equation (8) connects the applied force ($-\partial_i \rho$) with the flux (J_i). Such equations are called constitutive equations because they describe a physical property of the material. (The familiar Ohm's law $J = \sigma E$

is another example of this.) In addition to eq. (8), we also have the usual current conservation equation

$$\partial_\mu J^\mu = 0. \quad (9)$$

If D is constant, elimination of J_i gives

$$(\partial_0 - D\,\partial_i^2)\rho = 0.$$

This is the diffusion equation. It is parabolic. Its solution is

$$\rho \propto \exp(-x^2/4Dt)/\sqrt{4\pi D t}.$$

It is easy to see that the solution violates causality: Initially (i.e., in the limit $t \to 0$), this is the Dirac delta function. But at any finite time, howsoever small, it is nonzero everywhere, even outside the lightcone. Now eq. (9) cannot be wrong. So to restore causality the constitutive equation (8) which anyway was a hypothesis, is replaced by

$$\tau_J \partial_0 J_i + J_i = -D\,\partial_i \rho, \quad (10)$$

where τ_J is a parameter with dimensions of time. In eq. (8), if the force vanishes, the flux vanishes instantaneously without any time lag. In contrast, in eq. (10) the flux relaxes to zero exponentially. τ_J is called the relaxation time. The new diffusion equation is

$$\tau_J \partial_0^2 \rho + \partial_0 \rho - D\,\partial_i^2 \rho = 0.$$

This equation is hyperbolic and is called the Telegraphist's equation [84]. If $v^2 \equiv D/\tau_J < 1$, causality is restored.

Now consider hydrodynamics. The conservation and constitutive equations are

$$\partial_\mu T^{\mu\nu} = 0,$$

$$T_{ij} = P\,\delta_{ij} - \eta\left(\partial_i u_j + \partial_j u_i - \frac{2}{3}\delta_{ij}\partial_k u_k\right) - \zeta\,\delta_{ij}\partial_k u_k.$$

Here $T^{\mu\nu}$ is the energy-momentum or stress-energy tensor, P is the equilibrium pressure, and η and ζ are the coefficients of shear and bulk viscosity, respectively. Tensor decomposition is now more complicated. But the basic idea remains the same. Causality is restored by introducing higher-order terms in the gradient expansion. This forces introduction of a new set of transport coefficients, e.g., τ_π and τ_Π which are relaxation times corresponding to shear and bulk viscosities. They are important at early times or for a rapidly evolving fluid. For details, see e.g. [82].

4.4. Recent Results from Causal Viscous Hydro

The Israel-Stewart formulation [80] of the causal dissipative hydro is commonly used for numerical applications. However, it is not the only causal formulation available. There are others such as Müller's theory [79], Carter's theory [85], Ottinger-Grmela formulation [86], memory function method of Koide et al. [87], etc.

We have already mentioned the early work by Muronga [82]. Since then several authors have studied various aspects of the causal viscous hydro. We now describe briefly only a few of the most recent of these papers. This will also give the reader a feel for the complexities of these calculations and the uncertainties therein. (Other very recent papers which we shall not describe are listed in [88].)

Romatschke and Romatschke [89] used the Israel-Stewart theory. They assumed longitudinal boost invariance and used Glauber-type initial conditions. The initial shear pressure tensor $\pi^{\mu\nu}$ was assumed to be zero. η/s was treated as a fixed number independent of temperature. The bulk viscosity was ignored. For the EOS they used the semirealistic result of Laine and Schroder [90], and calculated the elliptic flow v_2. Their conclusion was that p_T-integrated v_2 is consistent with η/s up to 0.16; see Fig. 26. However, the minimum-bias $v_2(p_T)$ favoured $\eta/s < 1/4\pi$ violating the KSS bound [16]; see Fig. 27.

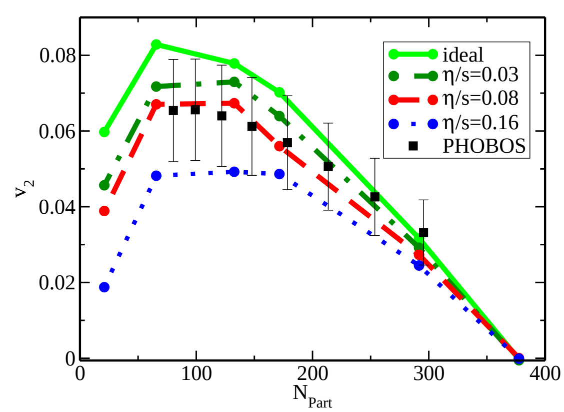

Figure 26. Au-Au, 200 GeV, p_T-integrated v_2 for charged particles vs number of participant nucleons. PHOBOS: 90% confidence level systematic errors. From [89].

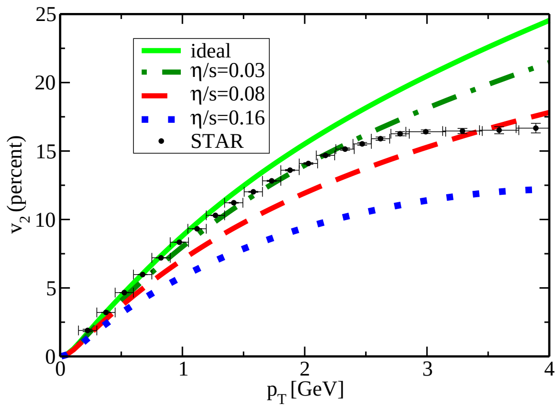

Figure 27. Au-Au, 200 GeV, minimum-bias $v_2(p_T)$ for charged particles. STAR: only statistical errors. From [89].

Dusling and Teaney [91] used the Ottinger-Grmela formalism of causal viscous hydro. They assumed longitudinal boost invariance and used Glauber-type initial conditions. The initial shear pressure tensor ^{ij} was taken to be $\partial^i u^j$ as in the Navier-Stokes theory. =s was treated as a xed number independent of temperature. The bulk viscosity was ignored. The EOS used by them was simply p = =3 without any phase transition. Their conclusion was that if the e ects of viscosity are included in the evolution equations but not in the freezeout, then the v_2 is a ected only modestly. If, however, they are included at both the places, then v_2 is signi cantly reduced at large p_T.

Why does the shear viscosity suppress $v_2(p_T)$? Shear viscosity represents a frictional force proportional to velocity. For an in-plane elliptic ow, the in-plane ow velocity is higher than that out of plane. So the in-plane frictional force is stronger. This tends to reduce the ow anisotropy and hence $v_2(p_T)$.

Calculations described above include the shear viscosity in some approximation, but ignore the bulk viscosity completely. What do we know about the bulk viscosity of the strongly interacting matter? In the high-temperature limit, pQCD calculations [92] give the following results for the shear and bulk viscosity coe cients

$$\frac{T^3}{{}_s^2 \ln {}_s^1} \quad \text{and} \quad \frac{{}_s^2 T^3}{\ln {}_s^1}:$$

As T increases, both and increase. However, the ratio = decreases showing the reduced importance of the bulk viscosity at high T. Also note that the entropy density s T^3, and hence =s increases with T, whereas =s decreases with T. This is easy to understand because QCD becomes conformally symmetric at high temperatures.

In the decon nement transition region the conformal symmetry is badly broken, and there is no reason to expect the bulk viscosity to be negligible. Extracting for temperatures in this region from lattice QCD is di cult; see section 2.4. However, some preliminary results are now available, and they indicate a dramatic rise of =s as T ! T_c [74].

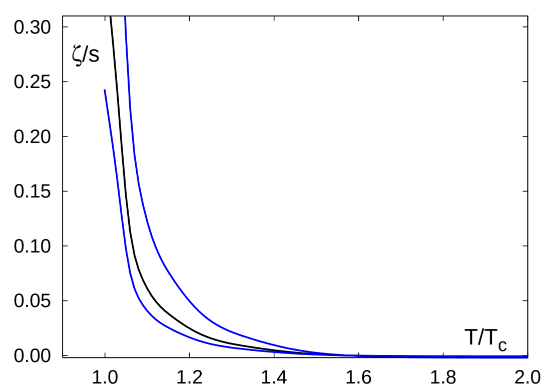

Figure 28. Bulk viscosity based on lattice data. $!_0$ = 0:5;1;1:5 GeV (top to bottom) is the scale at which pQCD is applicable. From [74].

Taking these results at their face value, Fries et al. [93] have studied the e ect of inclusion of the bulk viscosity in the hydro equations. They studied 1D expansion of the uid assuming longitudinal boost invariance. =s was held xed at 1=4 . A realistic EOS based on the lattice results of Cheng et al. [12] was used. Various initial conditions were tried. They concluded that (a) Large bulk viscosities around T_c lead to sizeable deviations from equilibrium throughout the entire lifetime of QGP. (b) Bulk viscosities just slightly larger than currently favoured could easily lead to breakdown of hydro around T_c. (c) The decreased pressure should slow down the expansion and increase the time spent by the uid in the vicinity of the phase transition. (d) The amount of entropy produced through bulk stress around T_c is smaller than that produced by shear stress at earlier times. Hence no large increase of the nal particle multiplicity is expected.

4.5. What Remains to be Done?

Bulk as well as shear viscosity (together with temperature dependence of ζ/s and η/s) needs to be incorporated.

Can causal viscous hydro with CGC-type initial conditions reproduce dN/dy, $\langle p_T \rangle$ and v_2 data? If so, what are the extracted η/s, ζ/s?

Causal viscous hydro + hadronic cascade is not done yet.

There are issues related to the hydro formalism itself. For example, Baier et al. [94] have recently shown that the Muller and Israel-Stewart theories do not contain all allowed second-order terms.

Present uncertainties in the hydro calculations limit the accuracy with which conclusions can be drawn. A coherent, sustained collaboration of experts in all stages of heavy-ion collisions is needed for a detailed, quantitative analysis of experimental data and theoretical models. Various numerical codes need to be compared with each other. To that end a new Theory-Experiment Collaboration for Hot QCD Matter (TECHQM) has been initiated. For details, see [95].

5. Predictions for LHC

Pb-Pb collisions at $\sqrt{s_{NN}} = 5.5$ TeV is an important part of the LHC experimental program. 5.5 TeV represents about 30-fold increase in the CM energy compared to the maximum energy explored at RHIC which in turn was about 10 times higher than that at SPS. Measurements on pp collisions as well as collisions of p, d, light ions with Pb will provide important benchmarks.

Among the experiments at LHC, CMS and ATLAS are primarily particle physics experiments/detectors, but they will study the physics of heavy-ion collisions too. ALICE (A Large Ion Collider Experiment), on the other hand, is a dedicated heavy-ion collision experiment. Physicists from several Indian universities and institutions have contributed in a big way to the ALICE collaboration. They are responsible for, among other things, the designing, testing, installation and maintenance of the Photon Multiplicity Detector (PMD) in ALICE and future upgrades of it. PMD is a preshower detector with fine granularity, full azimuthal coverage and one unit of pseudo-rapidity coverage. It will be used to measure the multiplicity, spatial distribution and correlations of produced photons on an event-by-event basis. Since photons escape the quark-gluon plasma without interactions, such measurements can potentially provide a cleaner glimpse of the early QGP phase. The Indian community has also made significant contributions to the muon spectrometer of ALICE. The spectromemter will be useful in the investigations of the J/ψ and other quarkonia, discussed in subsection 3.4. These particles are detected via their dimuon decay channel. The muon tracks will be found with an accuracy of better than one-tenth of a millimeter, thanks to the state-of-the-art readout electronics, known as MANAS, which was developed indigenously. ALICE has decided to use a Grid environment for their computing needs. India is a signatory to the Worldwide LHC Computing Grid and some of the Department of Atomic Energy installations are designated as Tier-II centers for this purpose.

A workshop was organized in 2007 at CERN in order to collect all the existing predictions for heavy-ion collisions at LHC. The proceedings [96] provide a broad overview of the field. Here we shall only present a few glimpses of what may be in store at LHC.

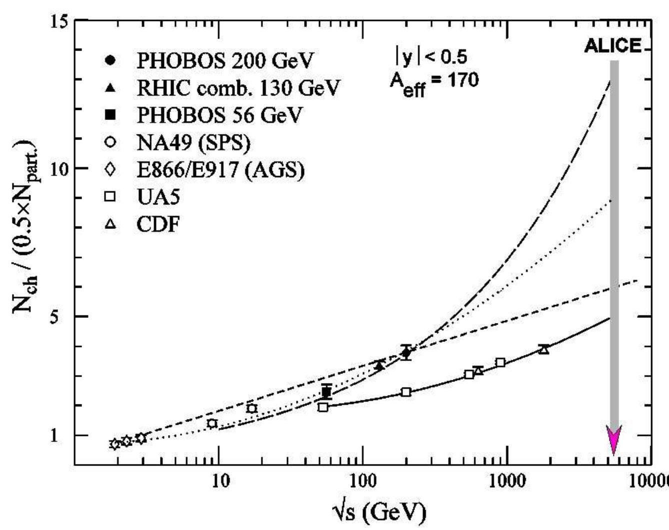

Figure 29. Charged-particle rapidity density per participant pair as a function of center-of-mass energy for AA and pp collisions. Dashed line: a fit linear in $\ln(\sqrt{s})$, Dotted curve: a fit quadratic in $\ln(\sqrt{s})$, Long-dashed curve: based on the saturation model of [97]. From [66].

One of the first and easiest measurements at ALICE would be that of the charged-particle multiplicity in the mid-rapidity region. Particle production models and simple fits which are in agreement with the AGS, SPS, and RHIC data on this quantity differ substantially from each other when extrapolated to the LHC energy,

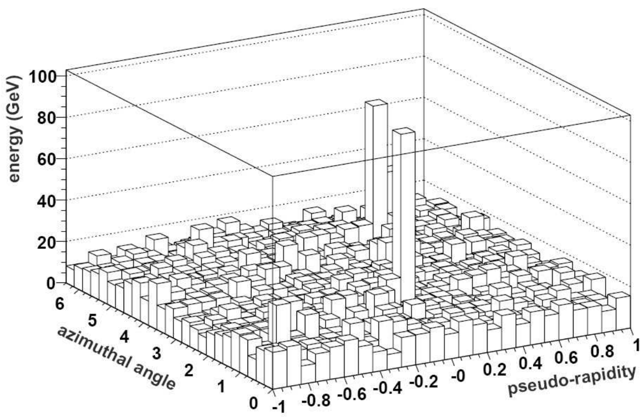

Figure 30. Pseudorapidity-azimuthal angle plot of Pb-Pb event at LHC energy with two 100 GeV jets generated with HIJING and PYTHIA event generators. From [98].

as shown in Fig. 29. Thus this simple "first-day" measurement will test our understanding of the physics of multiparticle production. The charged-particle multiplicity provides a handle on the initial entropy production; the latter quantity is a necessary input in the hydrodynamic evolution of the produced matter.

Another relatively simple measurement at ALICE would be that of the elliptic flow v_2 which has played a crucial role at RHIC (sec. 3.2). The initial energy density (eq. (4)) as well as the QGP lifetime are predicted to be higher at LHC than those at RHIC. This is expected to raise the value of $v_2(p_T)$. On the other hand, the increased radial flow at LHC is expected to lower it. (Recall the discussion on mass ordering in sec. 3.2.) The net effect on $v_2(p_T)$ depends on the mass of the hadron: Minimum-bias $v_2(p_T)$ for pions (protons) is expected to be higher (lower) at LHC than at RHIC, at low p_T; see Eskola et al. in [96]. Prediction by Kestin and Heinz is that $v_2(p_T)$ at a fixed impact parameter will be smaller at LHC than at RHIC, for pions as well as protons [96]. However, p_T-integrated elliptic flow is expected to be higher for all hadrons due to the increased relative weight at large values of p_T.

In sec. 3.5 we have quoted the values of T_{ch} and μ_B for the SPS and RHIC energies. The latest predictions for LHC are $T_{ch} = 161 \pm 4$ MeV and $\mu_B = 0.8^{+1.2}_{-0.6}$ MeV [96].

Hard processes: Cross sections for the production of heavy flavours, σ_{cc} and σ_{bb}, are expected to be about 10 and 100 times larger at LHC than at RHIC. Cross sections for the production of jets with transverse energy in excess of 100 GeV are expected to be several orders of magnitude higher. Jet-photon events will also be abundant. Figure 30 displays the capability of ALICE to reconstruct the high-energy jets at LHC in spite of the large soft-hadron background. Thus it would be possible to make detailed differential studies of heavy-quarkonium production, open-charm and open-beauty production, jet quenching, etc. at LHC [96]. It will also be possible to study quark mass dependence and colour charge dependence of the energy loss of a parton as it traverses the medium.

Thus LHC promises to be a valuable tool to test our models of ultrarelativistic heavy-ion collisions and deepen our understanding of QCD. For details, see [99].

REFERENCES

1. P.W. Higgs, Phys. Rev. Lett. 13 (1964) 508.
2. C. Amsler et al., Phys. Lett. B 667 (2008) 1.
3. P.V. Landshoff, arXiv:0709.0395.
4. U.M. Heller, MILC Collaboration, J. Phys. Conf. Ser. 9 (2005) 248.
5. W.-M. Yao et al., J. Phys. G 33 (2006) 1.
6. C. Aubin, et al., Fermilab Lattice, MILC and HPQCD Collaborations, Phys. Rev. Lett. 95 (2005) 122002.
7. M. Artuso et al., CLEO-c Collaboration, Phys. Rev. Lett. 95 (2005) 251801.
8. B. Aubert et al., BABAR Collaboration, Phys. Rev. Lett. 98 (2007) 141801.
9. Y. Aoki, G. Endrodi, Z. Fodor, S.D. Katz and K.K. Szabo, Nature 443 (2006) 675.
10. Y. Aoki, Z. Fodor, S.D. Katz K.K. Szabo, Phys. Lett. B 643 (2006) 46.
11. M. Cheng et al., Phys. Rev. D 74 (2006) 054507.
12. M. Cheng et al., Phys. Rev. D 77 (2008) 014511.
13. R.V. Gavai, S. Gupta and S. Mukherjee, Pramana 71 (2008) 487.
14. S. S. Gubser, I. R. Klebanov and A. A. Tseytlin, Nucl. Phys. B 534 (1998) 202.
15. A. Nakamura and S. Sakai, Phys. Rev. Lett. 94 (2005) 072305.
16. P. Kovtun, D T. Son, A.O. Starinets, Phys. Rev. Lett. 94 (2005) 111601.
17. H.B. Meyer, Phys. Rev. D 76 (2007) 101701.
18. R.V. Gavai and S. Gupta, Phys. Rev. D 73 (2006) 014004.
19. J. Cleymans, J. Phys. G 28 (2002) 1575.
20. V. Koch, A. Majumder and J. Randrup, Phys. Rev. Lett. 95 (2005) 182301.

21. O. Kaczmarek and F. Zantow, Phys. Rev. D 71 (2005) 114510.
22. M. Asakawa and T. Hatsuda, Phys. Rev. Lett. 92 (2000) 120014; S. Datta, F. Karsch, P. Petreczky and I. Wetzorke, Phys. Rev. D 69 (2004) 094507.
23. T. Matsui and H. Satz, Phys. Lett. B 178 (1986) 416.
24. M. Buballa, Phys. Rept. 407 (2005) 205.
25. K. Rajagopal and F. Wilczek, in "At the Frontier of Particle Physics / Handbook of QCD", Vol. 3, M. Shifman, ed., (World Scienti c), p. 2061.
26. L. McLerran and R. D. Pisarski, Nucl. Phys. A 796 (2007) 83.
27. R. V. Gavai, Phys. Rev. D 32 (1985) 519.
28. D. Banerjee, R. V. Gavai and S. Sharma, Phys. Rev. D 78 014506 (2008) and e-Print: arXiv:0809.4535 [hep-lat].
29. Z. Fodor and S. Katz, J.H.E.P. 0203 (2002) 014.
30. C. R. Allton et al., Phys. Rev. D 66 (2002) 074507; Ph. de Forcrand and O. Philipsen, Nucl. Phys. B 642 (2002) 290; M.-P. Lombardo and M. d'Elia, Phys. Rev. D 67 (2003) 014505. C. R. Allton et al., Phys. Rev. D 68 (2003) 014507; R. V. Gavai and S. Gupta, Phys. Rev. D 68 (2003) 034506.
31. R. V. Gavai and S. Gupta, Phys. Rev. D 71 (2005) 114014.
32. R. V. Gavai and S. Gupta, e-Print: arXiv:0806.2233 [hep-lat].
33. J. D. Bjorken, in Current Induced Reactions, Lecture Notes in Physics vol. 56, New York: Springer, p. 93.
34. J. D. Bjorken, Phys. Rev. D 27 (1983) 140.
35. T. Lappi and L. McLerran, Nucl. Phys. A 772 (2006) 200.
36. White paper by the STAR Collaboration, Nucl. Phys. A 757 (2005) 102.
37. M. Gyulassy, arXiv: nucl-th/0403032.
38. N. Borghini, P. M. Dinh, J. Y. Ollitrault, Phys. Rev. C 64 (2001) 054901.
39. N. Borghini, P. M. Dinh, J. Y. Ollitrault, Phys. Rev. C 66 (2002) 014905.
40. R. S. Bhalerao, N. Borghini, J. Y. Ollitrault, Phys. Lett. B 580 (2004) 157; Nucl. Phys. A 727 (2003) 373; N. Borghini, R. S. Bhalerao, J. Y. Ollitrault, J. Phys. G 30 (2004) S1213.
41. S. A. Voloshin, A. M. Poskanzer, R. Snellings, arXiv:0809.2949.
42. R. S. Bhalerao, J. P. Blaizot, N. Borghini, J. Y. Ollitrault, Phys. Lett. B 627 (2005) 49; H. J. Drescher, A. Dumitru, C. Gombeaud, J. Y. Ollitrault, Phys. Rev. C 76 (2007) 024905.
43. M. D. Oldenberg (for the STAR Collaboration), J. Phys. G 31 (2005) S437.
44. B. Muller, Acta Phys. Pol. B 38 (2007) 3705.
45. See, e.g, R. D. Field, \Applications of Perturbative QCD", Addison-Wesley Publishing Company, The Advanced Book Program, 1989; Yu. Dokshitzer, V. Khoze, A. Mueller and S. Troyan, \Basics of perturbative QCD", Edition Frontiers 1991.
46. C. A. Salgado and U. A. Wiedemann, Phys. Rev. D 68 (2003) 014008.
47. J. Adams, et al. (STAR Collaboration), Phys. Rev. Lett. 91 (2003) 072304.
48. J. Adams, et al (STAR Collaboration), Phys. Rev. Lett. 97 (2006) 162301.
49. R. Baier, D. Schi and B. G. Zakharov, Ann. Rev. Nucl. Part. Sci. 50 (2000) 37.
50. C. Loizides, Eur. Phys. J. C 49 (2007) 339.
51. A. Adare, et al. (PHENIX Collaboration), e-Print: arXiv:0801.4020 [nucl-ex].
52. F. Karsch and R. Petronzio, Phys. Lett. B 193 (1987) 105.
53. R. V. Gavai and S. Gupta, Phys. Lett. B 216 (1989) 239.
54. R. V. Gavai, S. Gupta and K. Sridhar, Phys. Lett. B 227 (1989) 161.
55. C. Gerschel and J. Hufner, Ann. Rev. Nucl. Part. Sci. 49 (1999) 255; Phys. Lett. B 207 (1988) 253.
56. R. Gavai, et al., Int. J. Mod. Phys. A 10 (1995) 3043.
57. B. Alessandro et al. (NA50 Collaboration), Eur. Phys. J. C 39 (2005) 335.
58. A. Capella and E. G. Ferreiro, Eur. Phys. J. C 42 (2005) 419 and references therein; E. L. Bratkovskaya, A. P. Kostyuk, E. Cassing and H. Stocker, Phys. Rev. C 69 (2004) 054903.
59. M. Gazdzicki and M. I. Gorenstein, Phys. Rev. Lett. 83 (1999) 4009.
60. A. Adare, et al. (PHENIX Collaboration), Phys. Rev. Lett. 98 (2007) 232301.
61. M. J. Tannenbaum, e-Print: arXiv:nucl-ex/0702028.
62. H. Satz, J. Phys. G 32 (2006) R25.
63. P. Braun-Munziger anf J. Stachel, Phys. Lett. B 490 (2000) 196; R. L. Thews, M. Schroedter and J. Rafelski, Phys. Rev. C 63 (2001) 054905.
64. J. Cleymans and H. Satz, Z. Phys. C 57 (1993) 135; P. Braun-Munzinger, I. Heppe, J. Stachel, e-Print: arXiv:nucl-th/9903010.
65. P. Braun-Munzinger, K. Redlich, J. Stachel, in Quark-Gluon Plasma 3, eds. R. C. Hwa and X. N. Wang, (World Scienti c, Singapore, 2004).
66. F. Carminati et al. [ALICE Collaboration], J. Phys. G 30 (2004) 1517.

67. A. Andronic, P. Braun-Munzinger, J. Stachel, Nucl. Phys. A 772 (2006) 167.
68. STAR Collaboration, Phys. Rev. C 72 (2005) 14904.
69. T. Hirano et al., Phys. Lett. B 636 (2006) 299; T. Hirano, Prog. Theor. Phys. Suppl. 168 (2007) 347; A. Adil et al. Phys. Rev. C 74 (2006) 044905.
70. O. Socolowski, F. Grassi, Y. Hama and T. Kodama, Phys. Rev. Lett. 93 (2004) 182301.
71. M. Miller and R. Snellings, arXiv:nucl-ex/0312008; B. Alver et al. [PHOBOS Collaboration], Phy. Rev. Lett. 98 (2007) 242302; R. S. Bhalerao and J. Y. Ollitrault, Phys. Lett. B 641 (2006) 260.
72. R. J. Fries, J. Phys. G 34 (2007) S851.
73. P. Huovinen, Nucl. Phys. A 761 (2005) 296.
74. F. Karsch, D. Kharzeev, K. Tuchin, e-Print: arXiv:0711.0914 [hep-ph].
75. L. P. Csernai, J. I. Kapusta, L. D. McLerran, Phys. Rev. Lett. 97 (2006) 152303.
76. P. Danielewicz and M. Gyulassy, Phys. Rev. D 31 (1985) 53.
77. C. Eckart, Phys. Rev. 58 (1940) 919.
78. L. D. Landau and E. M. Lifshitz, Fluid Mechanics (Pergamon, London, 1959).
79. I. Muller, Z. Phys. 198 (1967) 329; Living Rev. Relativity 2 (1999) 1.
80. W. Israel and J. M. Stewart, Ann. Phys. (N.Y.) 118 (1979) 341.
81. W. A. Hiscock and L. Lindblom, Ann. Phys. (N.Y.) 151 (1983) 466.
82. A. Muronga, Phys. Rev. Lett. 88 (2002) 062302; Phys. Rev. C 69 (2004) 034903.
83. M. Natsuume, arXiv:hep-ph/0701201; D. T. Son and A. O. Starinets, arXiv: 0704.0240; D. Mateos, arXiv: 0709.1523.
84. P. M. Morse and H. Feshbach, Methods of Theoretical Physics (McGraw-Hill, NY, 1953).
85. B. Carter, Proc. Roy. Soc. London, Ser. A, 433 (1991) 45; N. Andersson and G. L. Comer, Living Rev. Relativity 10 (2007) 1.
86. M. Grmela and H. C. Ottinger, Phys. Rev. bfE 56 (1997) 6620.
87. T. Koide, G. S. Denicol, P. Mota and T. Kodama, Phys. Rev. C 75 (2007) 034909.
88. P. Huovinen and D. Molnar, arXiv:0808.0953; M. Luzum and P. Romatschke, Phys. Rev. C 78 (2008) 034915; H. Song and U. W. Heinz, Phys. Rev. C 78 (2008) 024902; R. S. Bhalerao and S. Gupta, Phys. Rev. C 77 (2008) 014902; A. K. Chaudhuri, arXiv:0801.3180.
89. P. Romatschke and U. Romatschke, Phys. Rev. Lett. 99 (2007) 172301.
90. M. Laine and Y. Schroder, Phys. Rev. D 73 (2006) 085009.
91. K. Dusling and D. Teaney, Phys. Rev. C 77 (2008) 034905.
92. P. Arnold, G. D. Moore and L. G. Yaffe (2000); JHEP 05 (2003) 051; P. Arnold, C. Dogan and G. D. Moore, Phys. Rev. D 74 (2006) 085021.
93. R. J. Fries, B. Muller and A. Schafer, arXiv:0807.4333.
94. R. Baier et al., arXiv:0712.2451 (hep-th)
95. https://wiki.bnl.gov/TECHQM.
96. N. Armesto et al. (Editors), J. Phys. G 35 (2008) 054001.
97. K. J. Eskola et al., Nucl. Phys. B 570 (2000) 379.
98. K. Safarik, AIP Conf. Proc. 739 (2005) 346.
99. ALICE: Physics Performance Report, vol. I, J. Phys. G 30 (2004) 1517; vol. II, J. Phys. G 32 (2006) 1295.